multi-Risk sciEnce for resilienT commUnities undeR a changiNg climate

Codice progetto MUR: **PE00000005** – CUP LEAD PARTNER H93C22000610002

Deliverable title: Complements for multiple hazard scenarios from other vertical Spokes

Deliverable ID: 2.5.2

Due date: 15/03/2026

Submission date: 13/03/2026

AUTHORS

Luca Peruzzo (UNIPD), Giovanni Forte (UNINA), Lucia Mele (UNINA), Valeria Lo Presti (UNIPA), Diego Di Martire (UNINA), Silvio Coda (UNINA), Giorgio Cassiani (UNIPD), Domenico Calcaterra (UNINA), Francesca Bozzano (UNIROMA1), Francesco Silvestri (UNINA), Rosa Colacicco (UNIBA), Marco Bracci (UNIPA), Filippo Zaniboni (UNIBO), Scacchia Elena (ISPRA), Giovanni Poneti (OGS), Silvia Ceramicola (OGS), Daniele Spatola (UNIROMA1), Leonardo Maria Giannini (UNIROMA1), Carlo Esposito (UNIROMA1), Salvatore Martino (UNIROMA1)

Technical references

Project Acronym	RETURN
Project Title	multi-Risk sciEnce for resilienT commUnities undeR a changiNg climate
Project Coordinator	Domenico Calcaterra UNIVERSITA DEGLI STUDI DI NAPOLI FEDERICO II domcalca@unina.it
Project Duration	December 2022 – November 2025 (36 months)

Deliverable No.	DV2.5.2
Dissemination level*	
Work Package	2.5 - Outcomes for mitigation strategies
Task	1.4.3 – Complements for multiple hazard scenarios from other vertical Spokes
Lead beneficiary	UNIPD
Contributing beneficiary/ies	Luca Peruzzo (UNIPD), Giorgio Cassiani (UNIPD)

* PU = Public

PP = Restricted to other programme participants (including the Commission Services)

RE = Restricted to a group specified by the consortium (including the Commission Services)

CO = Confidential, only for members of the consortium (including the Commission Services)

Document history

Version	Date	Lead contributor	Description
0.0	16/09/2025	Luca Peruzzo	First draft
0.1	30/01/2026	Giorvanni Forte, Rosa Colacicco, Valeria Lo Presti, Luca Peruzzo, Salvatore Martino, Francesca Bozzano	Add Virtual Test Bed
0.2	12/03/2026	Valeria Lo Presti, Filippo Zaniboni, Daniele Spatola, Marco Bracci, Leonardo Maria Giannini, Luca Peruzzo, Giorgio Cassiani, Salvatore Martino, Francesca Bozzano	Add contributions from VS 2, marine and coastal environment
0.3	26/03/2026	Luca Peruzzo, Salvatore Martino	Links to RETURN Glossary, general review

ABSTRACT

This document summarizes the activities carried out within task 2.5.2, entitled “Complements for multiple hazard scenarios from other vertical Spokes”. The task contributes to the work package 5 “Outcomes for mitigation strategies” of the vertical spoke 2 on “Ground Instabilities” of the PE3 RETURN.

The work done for this deliverable followed the task description: Contribution to the development of multi-risk scenarios in synergy with spoke VS1 (for hydro-meteoric predisposing and triggering factors), VS3 (for seismic triggering factors). In particular, multi-risk scenarios of landslides at local/regional scale, including different triggering factors (VS3), volume estimation of mobilized material and effects of flash floods in submarine canyons (climate) (VS2). Information from satellite data analysis will also be provided (DV 2.5.2).

The task activities have been articulated in two parts. The first part focused on the review, selection and synthesis of the relevant contributions from the vertical spokes VS1, VS2, and VS3. This part also includes an introduction to the Virtual Test Bed developed within RETURN, and its use for the simulation of marine and terrestrial multi-risk scenarios The second part focused on the application of a selected tool chain to the assigned pilot case of Stigliano. This document opens with an overview of multi-hazard scenarios and multi-risk management, based on a review of the relevant literature and a summary of the activities and products of the RETURN partnership. The contributions considered include previous deliverables from spokes VS1 and VS3, additional documentation and proof of concepts.

Table of contents

Figures

1. Introduction

The study of ground instabilities and their dependency on predisposing and triggering factors of diverse nature aligns with multi-hazard and multi-risk perspectives that also look at the changing climate conditions. In the frame of this task and RETURN project in general, the multi-hazard perspective reflects the interplay and non-stationarity of predisposing, preparatory and triggering factors under a changing climate, as well the difficulty and danger in isolating individual processes and hazards. The distinction between predisposing, preparatory and triggering factors is made on a temporal basis: predisposing factors are considered invariable on the observation scale, while the preparatory factors show changes or cyclical trends during the same period. Lastly, a triggering factor is considered as a process that acts in a very short and well defined time (see DV 2.2.2 for a more detailed introduction of hazards factors).

The analysis of the interdependencies also extends to damage and impact scenarios, motivating a multi-risk perspective that acknowledges the ever growing connections between natural and societal elements at risk. Such a more comprehensive risk assessment has been supported also by the European Commission directives, specifically referring to the consideration of the interdependency among different hazards but also of the elements at risk (Maria Pia Boni et al., 2025). This interaction at the impact level is sometimes defined as level II interaction (a.k.a., consequence interaction), as distinguished from a level I of interaction, which is a multi-hazard scenario independent from the actual presence of elements at risk (Iannacone et al., 2024). Italy is characterized by a variety of multi-hazard environments, conditions that naturally arise from its geological, geomorphological, and hydrogeological complexity and heterogeneity (Prestininzi and Romeo, 2000).

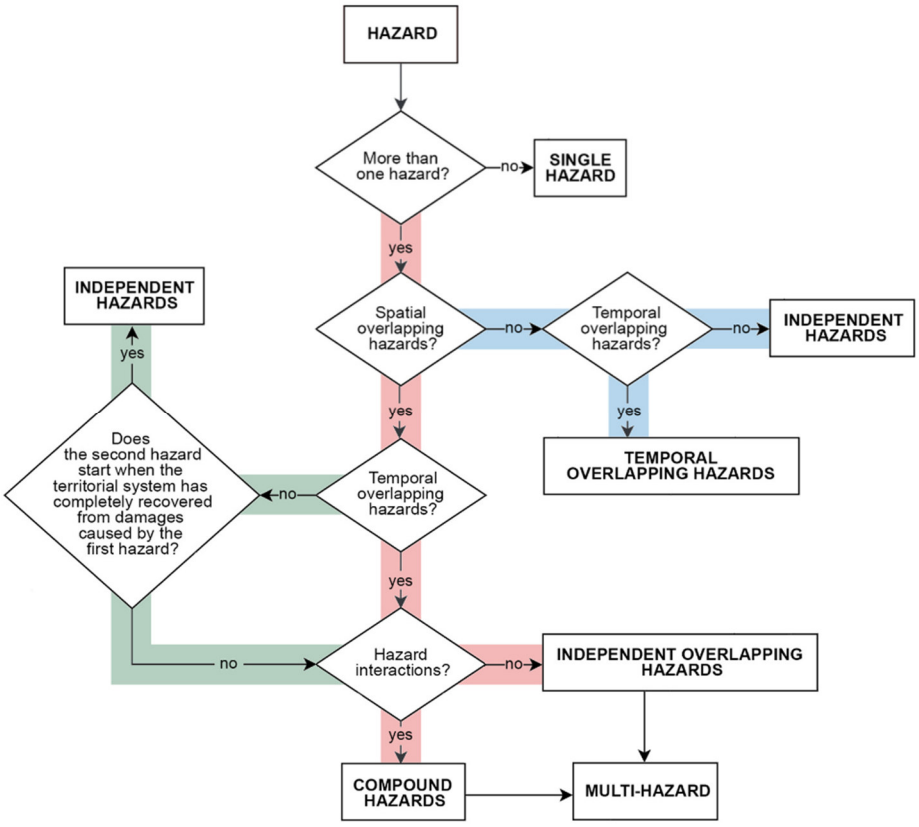

Figure 1. Conceptual framework for multi-hazard assessment, as recently presented by Boni et al., 2025.

The acknowledgment of interdependencies and unpredictability also aligns with a shift from probability to plausibility in a multi-hazard framework. This added perspective has been explored within the RETURN project, as it can resonate with stakeholders and the public, and thus represents an opportunity for improving awareness and engagement. Nonetheless, the shift from hazard to multi-hazard and multi-risk remains a challenge for the scientific community. For example, the concept of probability and uncertainty also has different implications within this shift. The complexity of multi-hazard and multi-risk has been propagated from conceptual models to the relevant tools.

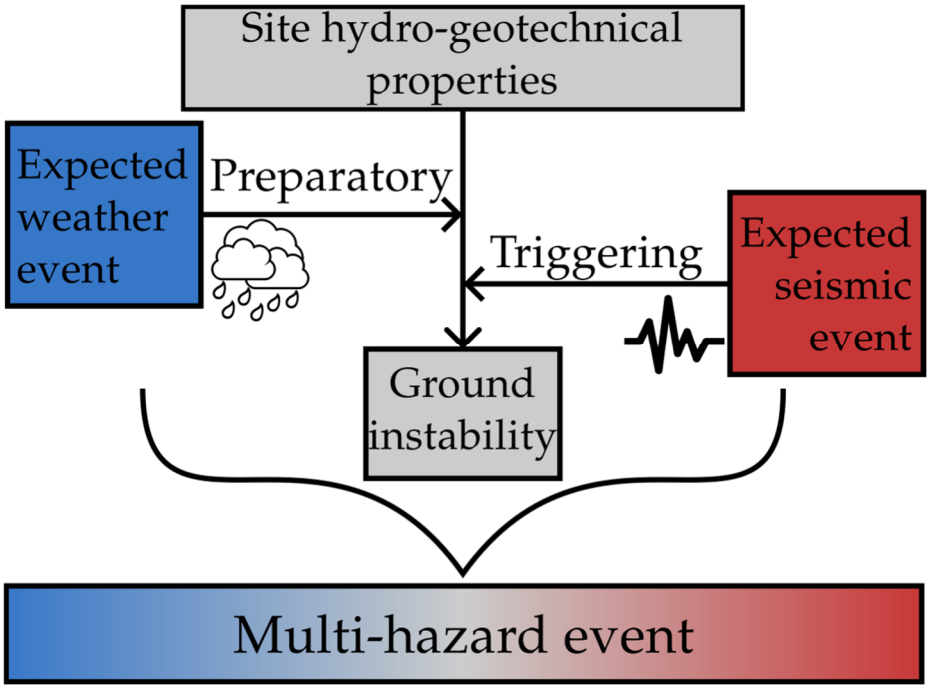

Figure 2. Frame for the multi-hazard scenario for weather-induced or earth-quake induced ground instabilities. The figure refers to the common scenario in which weather factors act as preparatory factors, while earthquakes are the triggering factors; however, the opposite or more complex scenarios are also possible.

When discussing multi-risk and the possibly associated shift to risk storylines, it is helpful to recall how the risk concept itself, central to any discussion, can assume slightly different connotations between popular and technical usages, as already recognized by the United Nations International Strategy for Risk Reduction (UNDRR, 2009). In technical usage, risk is the expected loss, with emphasis not only on the possibility of an event but also on the associated consequences, which is reflected in the well known combination of hazard, vulnerability and exposure. In popular usage, however, the emphasis is often on the probability, the chance, of an event. Similarly, the technical connotation of vulnerability may include the capacity, which defines the set of resources and skills that people and organizations have to cope with the event (resilience); however, in the popular usage, the term vulnerability more often and broadly includes and overlaps with the exposure. Certain terms may assume different meanings even within the multi-disciplinary technical framework involved in the multi-hazard assessment. Mitigation, for example, has a strong emphasis on prevention (i.e., reduction of greenhouse gas emissions) in the context of climate change; the emphasis necessarily changes when discussing earthquakes and landslides.

Multi-hazard scenarios involve and describe the co-occurrence of multiple hazards, which can be independent or connected by triggering – cascade effects. The multi-hazard scenarios represent the basis for consequent damage and impact scenarios, typically in this order, as damage refers to the direct - physical consequences, while impact expresses the aggregated effects / consequences of the event, which can be general or specific (economical, functional, human, etc.). Finally, risk is understood as an integrated assessment of possible damage and impact scenarios.

A brief literature review of weather- and earthquake-induced ground instabilities opens the specific sections on contributions from the VS 1 Water and VS 2 Earthquakes and Volcanoes. In the interest of brevity and Italian scope, particular attention was paid to the studies authored within the RETURN project or by RETURN authors in recent years.

1.1 Introduction to the Virtual Test Bed

The assessment of the complexity of the cause-effect relationship in natural processes, while enabling the evaluation of influencing factors and parameters, represents one of the main challenges in multi-risk scenarios. Through the integration of multidisciplinary expertise, the RETURN Project generated a Virtual Test Bed

(VTB) offering to the scientific community and stakeholders a scalable and territorially transposable approach to address this important issue. The RETURN VTB, called RETURNLAND, is a virtual complex mosaic of Italian territorial elements broadly representative of physiographic units and the geological processes active within them. This virtual environment is a Digital Terrain Model consistent with fundamental physiographic constraints (contiguity of reliefs and plains, drainage patterns, coastal development, etc.), while ensuring the territorial scalability of the representations. This virtual demonstrator was used to activate several tool chains capable of producing irreversible effects on the ground surface and in the submarine environment, which can be addressed, through impact chains, to damage infrastructure, urban areas, and communities. This task presents the part of the VTB that relates to the development and application of the tools for multi-risk scenarios.

2. Contributions from VS 1 - Water

Weather events (chiefly rainfall) and consequent alteration of the stability of the subsurface are widely recognized as major factors causing landslides and other ground instabilities. Water inputs can act as preparatory factors (weathering, groundwater changes, morphological changes, etc.) or as triggering factor by directly impacting the subsurface equilibrium between resisting and driving forces, for example increasing the pore pressure and thus reducing the shear strength, while also increasing the weight - driving forces (Guzzetti et al. 2020). The weather influence on the equilibrium conditions includes thermodynamic, hydraulic, and mechanical processes occurring at different spatial and temporal scales (Uhlemann et al., 2016). Rainfall often dominates the above processes: four rainfall parameters are commonly recognized: 1) total amount of rainfall, 2) short-term rainfall intensity, 3) antecedent rainfall; and 4) rainfall duration (Guzzetti et al., 2022).

The importance of weather events for ground instability has led to substantial specific literature on weather-induced landslides and related analyses of risk scenarios and mitigation strategies (Tagarelli and Cotecchia, 2025, and references therein). The implementation of weather-based early warning systems directly expresses the synergy between ground instability and weather monitoring and forecasting. These systems are typically divided into territorial and local. The territorial systems are characterized by the covered area, which typically includes multiple exposed sites. Because of the spatial scale and resolution of the monitoring, these systems can take advantage of existing weather stations and networks, while issuing specific warning to the different sites based on the estimated or forecasted weather conditions (Piciullo et al., 2020; Guzzetti et al., 2020). On the contrary, local systems serve a specific site and include ad hoc monitoring networks, possibly connecting both weather and surface/subsurface sensors. In fact, the meteorological monitoring alone does not consider critical soil properties controlling the initiation of the triggering process. Depending on these conditions, landslides may be triggered in response to a large variety of weather events. Although the integration of geotechnical monitoring (e.g., pore water pressure, soil water content, ground deformation) within warning models for weather-induced landslides may be challenging, it can provide additional information to determine the likelihood of rainfall events actually triggering failure (Pecoraro et al., 2021).

The vertical spoke 1 Water investigated several triggering and predisposing factors of ground instabilities. The products of Spoke 1 reflect the extent and relevance of such factors. For example, the deliverable "Development of a focused observation and validation strategy for floods in poorly observed systems" (D 1.2.1) presents a general framework for conducting post flood surveys, highlighting how flood events are expected to vary in frequency and intensity under climatic changes. The focus on the investigated hydro-morphological changes is a good example of the dynamics of the predisposing factors. In particular, the deliverable includes among the methods the reconstruction of the hydrological event, the analysis of the flood hydraulic variables, and analysis and mapping of the coupling/decoupling between landslides and channel hydro-morphological changes. Broadening the scope to multi-hazard and its associated complexity of spatiotemporal scales and processes, the deliverable also recognizes the analysis of the wood-vegetation dynamics and sedimentological changes. As it is well known, all these aspects play an important role in ground instabilities. While the deliverable focused on small-medium mountain basins, it has important contributions to important risk aspects that are present when considering the multi-scale and multi-risk approach encouraged by RETURN and central to the present task.

Suitable data management (integration, accessibility, and automation) is fundamental in multi-hazard and multi-risk. In this regard, Spoke 1 developed two important information systems named ATLAS (nATional fLood informAtion System), EXTRAFLOOD (EXTreme RAinfall and FLOOD projections over Italy) and NatFIM (National Flood Impact Model). The information and functionalities can contribute in multiple ways to multi-risk. The statistical analysis and nowcasting of precipitations are central to hydrometeoric predisposing and triggering factors. In addition, ATLAS can also include surface information regarding site general conditions and damage assessment. Thanks to this coupling of hydro-meteoric and geomorphological information, ATLAS can positively contribute to the multi-hazard and multi-risk management, including early-warning capabilities. Always about the coupling of hydro-meteoric and geomorphological aspects, EXTRAFLOOD directly focuses on the analysis and projection of the changes associated with climate dynamics. EXTRAFLOOD integrates existing and novel methodology that directly address the dramatic relevance of storms, floods and associated ground instabilities. While challenging, EXTRAFLOOD also

accounts for short hydro-meteoric events and ensuing hazards, reflecting their actual relevance and riskiness (see DV 1.2.2 and references therein). Relative to ATLAS and EXTRAFLOOD, NatFIM targets more specifically floods and their impact. It aims to assess the impact of flood scenarios (reconstructed or simulated), given the relevant spatiotemporal information of the flood event, e.g., water levels, velocities and residence times, and distribution exposure and vulnerability. Both spatiotemporal information and analyses are designed to function in a GIS environment to ease the product adoption and reusability. In this sense, while it is largely flood-specific, some key functionalities can contribute to multi-risk management. See deliverable 1.2.3 "Identification, collection and preprocessing of available data sources and analysis of hazards, exposure, vulnerability and damage under the effects of global climate change" for a more in depth overview on ATLAS and NatFIM.

With regard to submarine flash floods, deliverable 1.4.2 reviewed the data and services available through MeteOcean and the historical national networks for sea level (Reta Mareografica Nazionale) and waves (Rete Ondametrica Nazionale). In addition to these well-established and long-term resources, there are also newer solutions for sea monitoring, such as the use of satellite imaging and coastal radars. While these resources often do not have the temporal and spatial coverage provided by the national networks, their capabilities can adapt to specific sites and projects, including areas where submarine ground instabilities may be expected and associated with relevant risk. The "National Coastal Evolution Tool" is a general initiative from the VS1 aimed at homogenizing the diverse sources of datasets on the coastline erosional or accretion trends, coupling such datasets with relevant functionalities to streamline the commonly desired processes (DV 1.4.1). Finally, at small spatial scales, cameras provide a powerful and versatile solution for real-time monitoring. Advanced quantitative information can be extracted from the images regarding coastal erosion, flooding events, vegetation dynamics, and riverine inputs of water and sediments. At the same time cameras are typically more economical than previous solutions, and their image can also provide a more qualitative but direct and general feedback. Together, installation ease and accessibility are conducive to a larger public engagement, which in turn can benefit more specific and technological investment, including submarine instrumentation and networks. Such technological advances show a significant overlap with existing systems for the monitoring of ground instabilities and thus can represent a meeting point and source of contributions.

3. Contribution from the VS 2 - Ground instabilities

3.1 Marine and Coastal environment

In marine environments, multiple hazards arise from the coexistence of different processes, such as submarine landslides, earthquakes and tsunamis, that can impact the same area, increasing the overall level of risk. A toolchain workflow was developed and applied to the VTB (Fig. 3). The toolchain consists of a sequence of processes starting from a submarine area where active fluid seepages are present. These structures predispose the sediments to potential instability by altering the geotechnical properties of the sediments. The workflow simulates the occurrence of a geological trigger - an earthquake - which destabilises a submarine landslide connected with the pockmark structures. A tsunami is generated by the landslide and the wave impact on the coast determines a coastal flooding scenario. This workflow also quantifies the Factor of Safety (FoS) for the area object of the investigation.

The tool chain description is provided in Deliverable 2.4.2: “Near shore and coastal areas, volcanic islands: thematic maps inducing hazard severity indicators and zoning for coupled/combined triggers.” A quantitative example is reported in this deliverable.

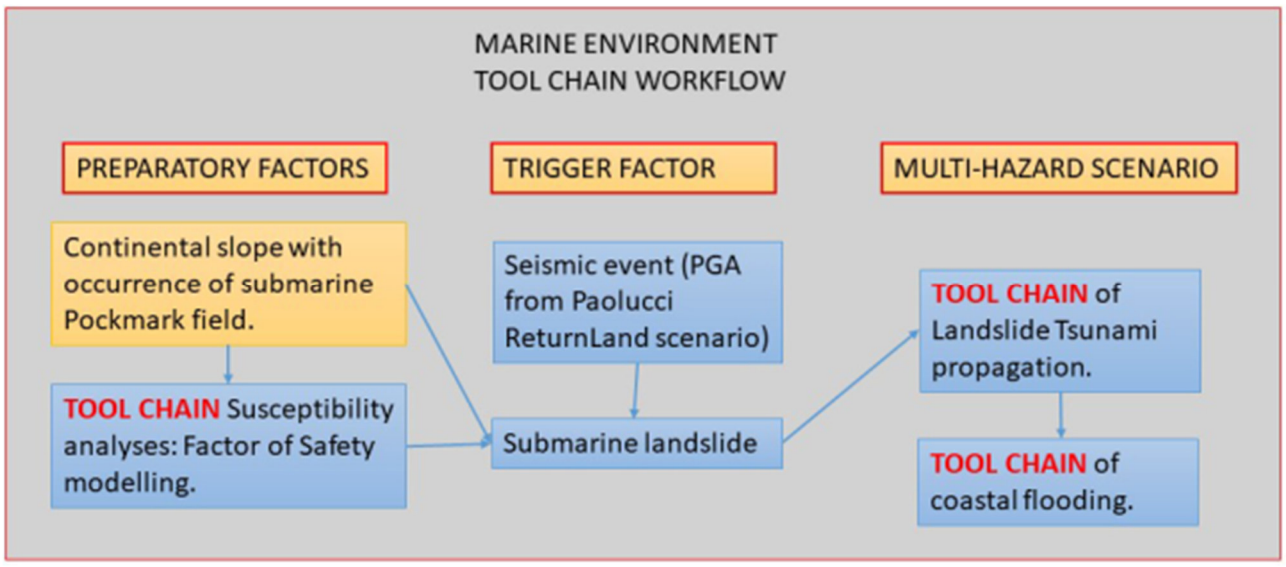

Figure 3. Toolchain workflow for rapid landslides in marine environments.

3.1.1 Submarine Pockmark

King and MacLean (1970) first introduced the term pockmark after recognizing and mapping these negative seabed features along the Nova Scotian shelf using early echo-sounder records. Since this pioneering work, pockmarks have been widely recognized as seabed depressions generated by focused subsurface fluid flow and escape (Hovland et al., 2002; Figs. 4, 5), and are now considered among the most ubiquitous geomorphological expressions of fluid venting on the seafloor (Dimitrov and Woodside, 2003; Hovland et al., 2002; Hovland and Svensen, 2006; Judd and Hovland, 2007).

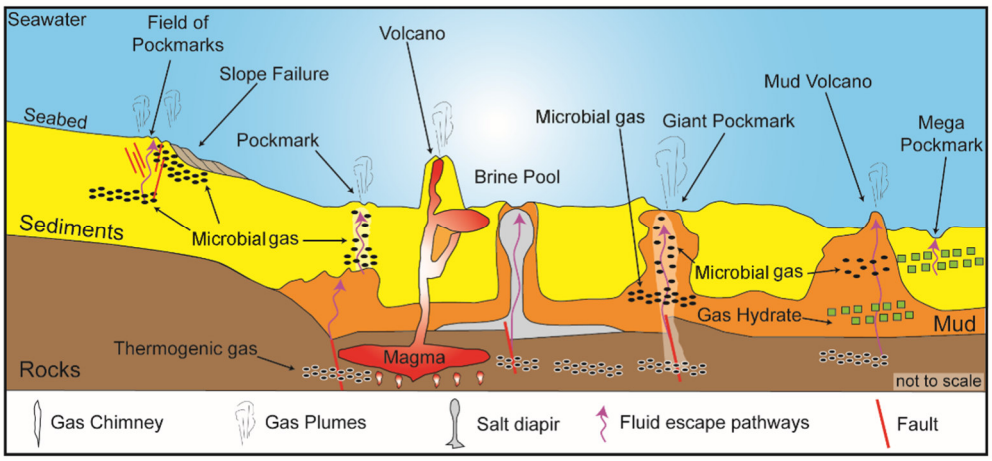

Figure 4. Simplified conceptual cartoon summarizing typical fluid-flow processes, associated seabed morphologies (e.g., pockmarks, mud volcanoes, brine pools), acoustic anomalies in the water column and sub-seabed, and potential fluid sources. (Spatola et al. 2025a).

In the literature, the term pockform was introduced by Iglesias et al. (2010) to describe pockmark-like seabed features linked to fluid escape but genetically associated with tectonically controlled or dissolution-induced collapse structures, as well as erosional morphologies such as scours and relict channel remnants. This terminology highlights the morphological continuum between fluid-related depressions and broader seabed instability processes.

Pockmarks display a wide range of sizes and morphologies, with diameters reaching several kilometres and depths up to ~150 m. They commonly show circular to elongate plan-view geometries, steep flanks, and flat- to cone-shaped bottoms (Ceramicola et al., 2018; Ho et al., 2012; Hovland et al., 2002; Judd and Hovland, 2007; Micallef et al., 2022; Pilcher and Argent, 2007). Bottom currents may play a fundamental role in their formation and/or post-formation modification (Picard et al., 2018), and elongated or aligned pockmarks are frequently interpreted as the result of current-driven erosion. In this context, the preferential orientation of elliptical, elongated, or chain-like pockmarks often coincides with contour-current directions, allowing their use as proxies for reconstructing near-bottom circulation patterns (Cattaneo et al., 2017).

Freshly formed pockmarks are typically maintained by prolonged, low-intensity seepage episodes, potentially driven by tidal forcing or localized bottom currents (Hammer et al., 2009; Pau et al., 2014). The internal slopes of pockmark walls average ~9°, with values commonly ranging between 6° and 18° (Fader, 1991). According to Pilcher and Argent (2007), newly formed pockmarks are likely conical depressions that progressively evolve toward rounded or flat-bottomed morphologies due to wall slumping and hemipelagic sediment infill. These gravitational reworking processes directly link pockmark evolution to small-scale mass wasting and sediment instability.

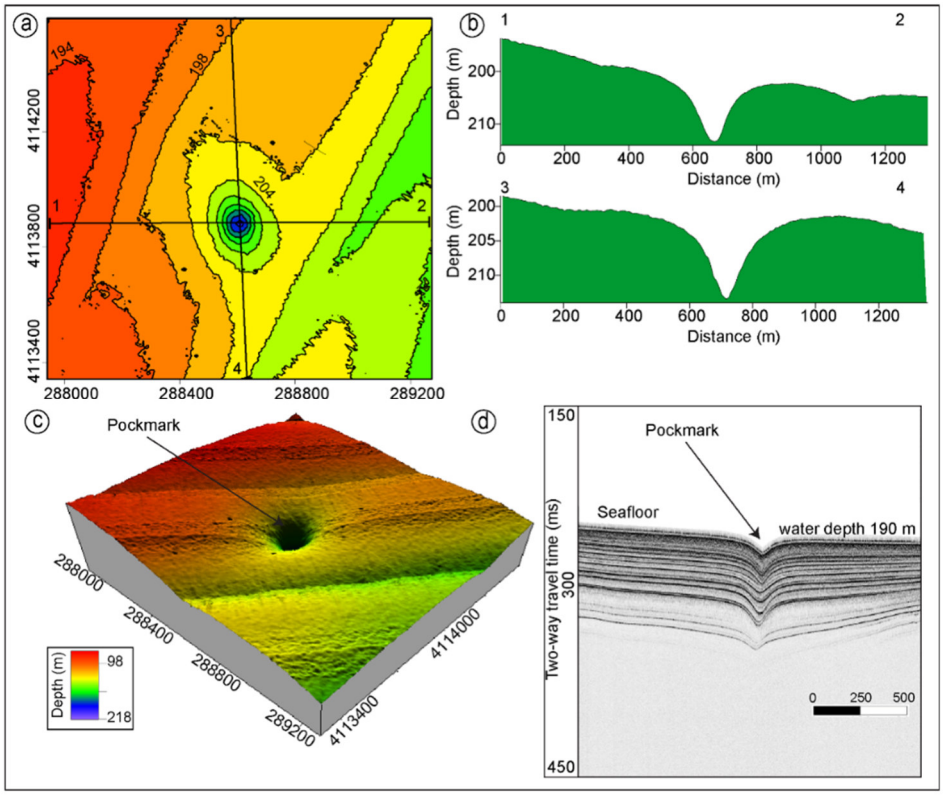

Figure 5. (a) Bathymetric map of a circular pockmark mapped on Graham Bank (Sicily Channel, southern Mediterranean Sea). (b) Bathymetric profiles across the pockmark centre. (c) 3D bathymetric model. (d) Chirp sub-bottom profile showing the internal seismic character of the pockmark (Spatola et al., 2025b).

Based on their morphological characteristics, pockmarks have been subdivided into different classes (Hovland et al., 1984; Hovland et al., 2002). The term unit pockmark was introduced by Hovland et al. (1984) to describe very small seabed depressions (1–10 m in diameter and up to ~0.6 m deep), occurring either in isolation, in clusters, or in association with larger pockmarks. In contrast, "normal" pockmarks typically range from 10 to 700 m in width and may reach depths of up to ~45 m. Unit and small normal pockmarks are often arranged in linear strings extending for kilometres, commonly aligned along zones of mechanical weakness in the shallow sedimentary cover, such as near-vertical faults, fractures, or flexures (Hovland et al., 2002). These alignments emphasize the strong structural control exerted by fluid pathways that may also act as preferential planes for slope failure initiation.

Pockmarks with diameters exceeding ~250 m are commonly referred to as giant pockmarks (Foland et al., 1999), first described on the Californian margin. Their spatial distribution may be clustered, random, or strongly controlled by underlying geological structures, including fault systems (Chand et al., 2014; Ingrassia et al., 2015; Judd and Hovland, 2007; Micallef et al., 2019; Pennino et al., 2014; Roy et al., 2019).

Over the last decades, pockmarks have been documented across all oceans, from continental shelves to abyssal plains, within a wide variety of geological and tectonic settings, including active and rifted continental margins, compressional regimes (subduction zones), and highly sedimented environments such as deltas (Brothers et al., 2012; Hovland, 2002; Hovland and Judd, 1988; Pilcher and Argent, 2007; Skarke et al., 2014). Buried pockmarks have also been identified in the stratigraphic record, locally reaching diameters of up to ~4 km, providing clear evidence of past episodes of focused fluid expulsion (Andresen et al., 2008; Ho et al., 2018). Depending on present-day activity, pockmarks can be classified as active—when ongoing gas or fluid venting is observed (Camerlenghi et al., 2019)—or inactive/dormant (Nickel et al., 2012).

Pockmarks are particularly abundant in hydrocarbon-rich provinces (Hovland et al., 1984; Rise et al., 1999; Zhu et al., 2020), areas where crystalline basement rocks subcrop beneath thin sedimentary covers, estuaries and coastal zones (García-García et al., 1999; Hill et al., 1992), regions characterized by high groundwater fluxes (Bussmann and Suess, 1998), and lacustrine environments, both with and without hydrothermal activity (Pickrill, 1993). Importantly, pockmarks are frequently observed in close spatial association with slope sedimentary failures and submarine landslides (Hovland et al., 2002; Riera et al., 2022), and in some cases

may act as precursors or focusing points for incipient channel development (Gay et al., 2007; Yu et al., 2021; Casalbore et al., 2022).

The close relationship between pockmarks, fluid overpressure, and sediment weakening implies a significant role in slope instability processes. Fluid escape reduces effective stress within the sediment, promotes shear-strength reduction, and may facilitate failure along pre-existing discontinuities, thereby enhancing the susceptibility of continental slopes to landsliding. For this reason, pockmarks are increasingly regarded as key indicators of potentially unstable seabed conditions and as relevant geohazards (Cox et al., 2020). Their presence has important implications for offshore infrastructure planning, the petroleum industry, and quantitative hazard assessment (Deville et al., 2020; Hovland et al., 2002; Lo Iacono et al., 2011; Szpak et al., 2012).

Finally, several geophysical observations suggest a potential link between pockmark activity and seismic processes. Variations in seawater temperature preceding earthquakes and persistent post-seismic gas venting from pockmarks have been reported (Dando et al., 1995; Hasiotis et al., 1997; Soter, 1998), supporting the existence of a close coupling between fluid migration and seismicity. Fluids are known to act as lubricants along fault planes, reducing friction and potentially facilitating fault slip (Kanamori and Brodsky, 2001), further reinforcing the role of pockmarks as surface expressions of deeper processes controlling both seismic activity and submarine slope instability.

3.1.2 Tsunami and coastal flooding

Landslide-tsunamis are very complex phenomena, since they involve chaotic and highly non-linear processes both in the generation phase (the mass-water interaction) and at the coast, where another interface (water-dry land) is found. Among the different approaches found in the scientific literature, encompassing a growing capability of treating and comprehending these phenomena with the aid of more sophisticated models and computational capacities, the use of parametric expressions represents a tool for fast estimation of waves generated by potential collapses, which can drive more detailed studies to specific cases or scenarios, which are worth of a dedicated effort.

In the framework of the vertical spoke VS2 – Ground Instabilities, two methodologies have been developed to assess the effects of a submarine landslide on the coast, in terms of maximum tsunami amplitude, and the consequent dry land flooding. These tools have already been extensively described in a previous deliverable (see DV 2.4.2 – Near Shore and coastal areas, volcanic islands: thematic maps inducing hazard severity indicators and zoning for coupled/combined triggers), and are then briefly reprised here.

The first one, called Landslide-Tsunami Tool, implements a parametric relation putting in relation some geometrical features of the landslide body (volume, V; initial depth of detachment, D; initial slope, θ; distance from the coast, d) to one of the most used metrics in the field of tsunami hazard assessment, i.e., the maximum wave amplitude at the coast, η. The equation reads:

$$\eta = A(V^{\varepsilon_V} \cdot D^{\varepsilon_D} \cdot d^{\varepsilon_d} \cdot sin\theta^{\varepsilon_\theta}) + B \qquad (1)$$

The exponents ε_V, ε_D, ε_d, ε_θ and the parameters A and B have been retrieved through a best-fit procedure adopting as a reference the results of numerical modelling applied to a set of landslide-tsunami scenarios to the case of Assi landslides (Ceramicola et al., 2014). Their values, obtained for two different types of environments (open slope, OS and canyon head, CH), are reported in Table 1.

Table 1. Values for the coefficients governing Eq. (1) obtained for the two different contexts (open slope and canyon head).

Parameter	OPEN SLOPE	CANYON HEAD
ε_V (Volume)	1.0	0.9
ε_D (Depth)	-1.2	-0.5
ε_d (Distance)	-0.5	-1.2
ε_θ (Slope)	1.1	0.5
A (Best fit)	0.01096	0.10543
B (Best fit)	-0.01328	0.00280

The second tool deals with dry land flooding, once the wave height at the coast is known. The procedure evaluates the height of the water column and its velocity along a topographic transect which origin is placed on the coast. The method implements the Energy Method (Kriebel et al., 2017), which bases on considerations about flow energy dissipation, due to the topographic slope and to the friction between the water and the inundated surface (this last contribution quantified by the Manning's roughness coefficient). In this way, it is possible to assess, for each point of the coastal area affected by the inundation, the impact of the tsunami. These two tools can be applied both in sequence, the first providing the input to the second, and singularly.

3.1.3 Factor Of Safety (FOS)

Factor of safety is defined as a margin of security against a risk, indicating how much stronger a part is than its usual loading. The current definition of the Factor Of Safety (FOS) is the ratio of the resistance of the system to the driven loading, in our case in the fluid escape pressure.

Herein, it is computed by the maximum factor that reduces the strength of materials up to the limit equilibrium.

In geology, the study of the safety factor related to slope stability uses highly specific geotechnical models. These models consider, as the acting physical elements, the resisting (stabilizing) forces that oppose the system's tendency to fail (e.g., a volume of sediments), and the driving (destabilizing) forces that instead tend to trigger or increase the likelihood of a landslide.

The comparison between these two systems of forces provides a deterministic indicator of stability through the Factor of Safety, which represents the ratio between stabilizing and destabilizing forces. Therefore, if FOS > 1, the system is considered stable; if FOS = 1, the system is in a condition of limit equilibrium; and if FOS < 1, the system is unstable.

In marine environment the identification of areas and volumes of altered sediments allows to develop not only a qualitative model regarding the potential future evolution of a submerged areas but also a quantitative study based on the calculation of the Factor of Safety (Noda et al., 2013; Sultan et al., 2004). This approach enables the study of the controlling parameters for the slope's evolution. In this case study, it is the pore overpressure in intra-pockmark area (Δu_{AFS}), and its threshold value, that determines the equilibrium of the slope.

The value of the Factor of Safety related to the variable Δu_{AFS}, reveals the potential role of submarine landslides whose volume could play a crucial role to generate tsunami waves and consequent coastal geohazard. To quantitatively assess the seabed stability related to the presence of pockmarks, the model proposed by Skempton and DeLory (1957) was chosen to compute the Factor of Safety. We modified it to suit the case study and to include the injection of fluids from the pockmark feeding system (considered 'external to the system' water column - sediment). The approach from the literature is a one-dimensional infinite slope model:

$$FOS_{static} = \frac{(10^3\gamma' h\alpha - \Delta u - \Delta u_{AFS})tantan\ \varphi + 10^3 c}{10^3\gamma' hsinsin\ \alpha\ coscos\ \alpha}\ ;\ FOS_{eq} = \frac{(10^3\gamma' h\alpha - \Delta u - \Delta u_{AFS})tantan\ \varphi + 10^3 c}{(10^3 k_h \alpha)10^3\gamma' hsinsin\ \alpha\ coscos\ \alpha}$$

The pore overpressure Δu is calculated according to the relationship by Sultan N. et al. (2004):

$\Delta u = \frac{10^6\ h\ S}{200}.\ \Delta u_{AFS}$ (Active Fluid Seepage)

is the contribution to the pore overpressure from the emission fluids from the pockmarks which is calculated using the inverse Hagen-Poiseuille law formula:

$\Delta u_{AFS} = \frac{8Q\eta L}{\pi R^4} - \rho g b - 101325Pa.$

For each variable present in the equations provided, a raster was produced to solve the equations in a GIS environment (using the raster calculator tool in QGIS) and, finally, to create a map of the FOS (the subscripts "static" and "eq" indicate static and pseudostatic conditions respectively). Regarding the production of the raster relating to ΔuAFS, whose value can be theoretically measured directly (despite the difficulties imposed by technological limits), it was estimated by imposing geometric parameters of the pockmark supply conduit (Q = volumetric flow rate of the fluids, L = length of the rising conduit, R = conduit of the duct assumed to be cylindrical) extrapolated from the seismic reflection profiles and from the multibeam data.

The Factor Of safety for this case study is calculated utilizing Parsifal-2 tools. It represents a new version of PARSIFAL enabling its adaptation and interconnection with the ReturnLand VTB. The acronym "PARSIFAL" was coined later and stands for probabilistic approach to provide scenarios of earthquake-induced slope failures (Della Seta et al., 2017, Martino et al., 2018, Martino et al., 2020). This new version of PARSIFAL, while preserving the structure and philosophy of the original project, introduced some substantial changes as the implementation of a model for assigning numerical indices linked to topological relationships between geometries (pixels) with specific FOS values and potentially vulnerable elements; this was introduced to allow the use (also) of an additional weight for FOS values. In addition to these two aspects, compared with the first PARSIFAL version, a model was introduced to provide landslide-hazard scenarios in a submarine environment. From a more formal standpoint, mainly related to the software code, this version of PARSIFAL involved a general rewrite of the code, allowing, among other things, the avoidance of dependencies on QGIS libraries, thus making the code usable independently of the development environment. All the code was written in Python, using standard libraries and/or implementing dedicated functions specifically developed for this project.

The geomechanical parameters applied to the case study are processed using the definition of the Factor of Safety (FOS) proposed by Skempton and DeLory (1957), in order to assess the threshold values of the geomechanical variables (e.g., intergranular cohesion, internal friction angle, undrained shear strength, etc.), and thus predict the response of the affected geological volume.

3.1.4 Simulation tools of marine and coastal area on the RETURN digital ecosystem including the RETURNLAND Virtual Test Bed

Today, the three tool chains constitute an important workflow that has been validated in RETURNALD Virtual Test Bed (https://zenodo.org/records/18987490).

This validation made it possible to simulate a coastal multi-hazard scenario involving both the coastal RETURNVILLE and the adjacent coastal plain, with the geological input originating from a landslide process that occurred in a submerged environment where there is an important pockmark field (Fig. 6).

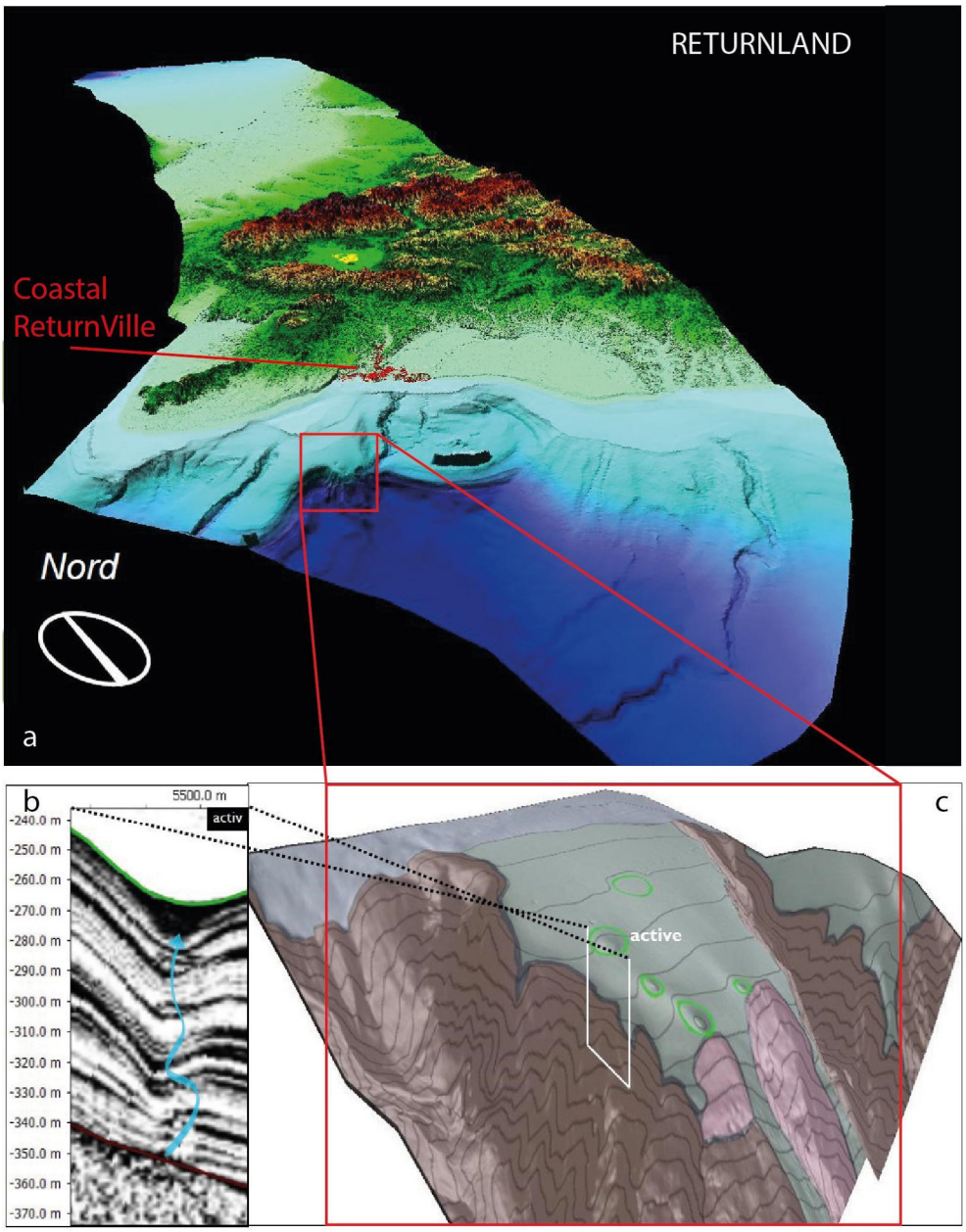

Figure 6. a) RETURNVILLE; the red square highlights the submarine area where a pockmark field is present; b) seismic profile in which it is possible to recognize the seismic facies typical of a fluid escape feature from the seafloor (the blue arrow indicates the direction of fluid migration); c) 3D multibeam data highlighting the submarine morphologies: pockmarks (green circles), canyon heads, and submarine landslides.

Using the Parsifal-2 modeling, which applies the FOS formula identified for the submerged sectors affected by fluid escape processes along with all the geotechnical parameters determined for the specific case, a susceptibility map of the analyzed marine area is obtained with the following FOS values (Fig. 7). The modeling shown in the image indicates that the most susceptible areas are the canyon heads and the pockmark areas, in particular the pockmark located at the shallowest depth.

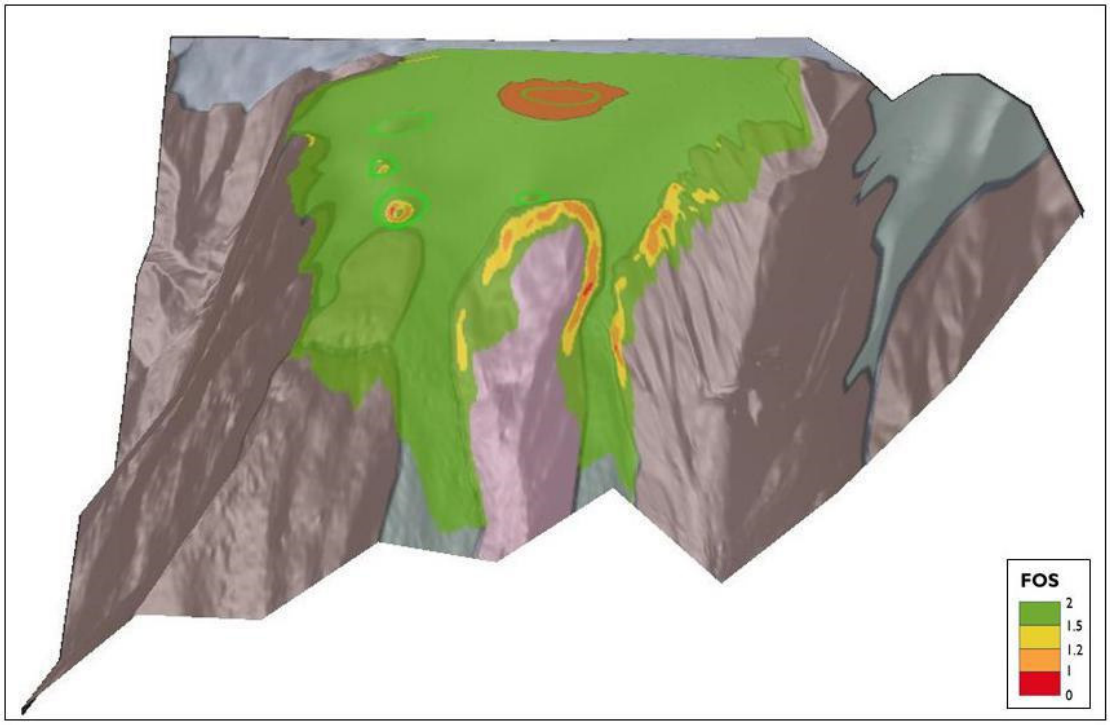

Figure 7. FOS values representation obtained from Parsifal-2 modelling on submarine area.

The workflow presented here analyzes a chain of impacts originating from this susceptibility assessment. The occurrence of a seismic trigger, whose PGA value is the same as that already applied to the RETURNALD VTB in the onshore environment (from the considered shaking map for RETURNLAND seismic scenario), acts as the driving mechanism for the initiation of submarine landslides.

Two landslide scenarios have been considered, one for each subaqueous environment: Open Slope (OS) area and Canyon Head area (CH). Table 2 reports their morphology in terms of volume, depth and slope. Notice that the OS case shows bigger volume, two orders of magnitude higher than the CH one, while the latter is characterized by steeper slope and smaller initial depth: all these features reflect the typical characteristics of landslides in the respective domains. Those parameters constitute the input for Eq. 1, together with the parameters listed in Table 1.

Table 2. Morphological characteristics of the landslide scenarios in the two considered environments (V, volume; D, initial depth; θ, initial slope).

Quantity	Units	Open Slope	Canyon Head
V	$10^6\ m^3$	94.3	0.84
D	m	120	20
θ	°	3	15

Figure 6a reports the positions of the two sources, OS and CH, marked respectively by the black and the red triangles. The landslide–tsunami model is applied to a series of points distributed along the coastline. For each point, the distance d from the source is calculated, allowing the expected wave amplitude to be estimated for each landslide scenario. Figure 6b shows the results, depicted in terms of cumulative distance along the shoreline starting from north. As expected, the OS case (in black) provides the higher signal, with a maximum of 1.4 m north of Returnville (in green) and an averaged amplitude of 1.2 in the urbanized coastal stretch - level that, though not catastrophic, is capable of dragging people into the water and could generate strong harbor currents, potentially damaging boats and triggering local resonances that could in turn amplify the tsunami effects. Notably, the wave impact is widespread across the entire analyzed coastal stretch, extending over 80 km, with amplitudes exceeding 60 cm. In contrast, the CH scenario produces much more localized waves, which maximum is around 30 cm in the closer portion of the RETURNVILLE coastal stretch. In this case, the tsunami effects are largely confined to the urban coastal area and negligible beyond it.

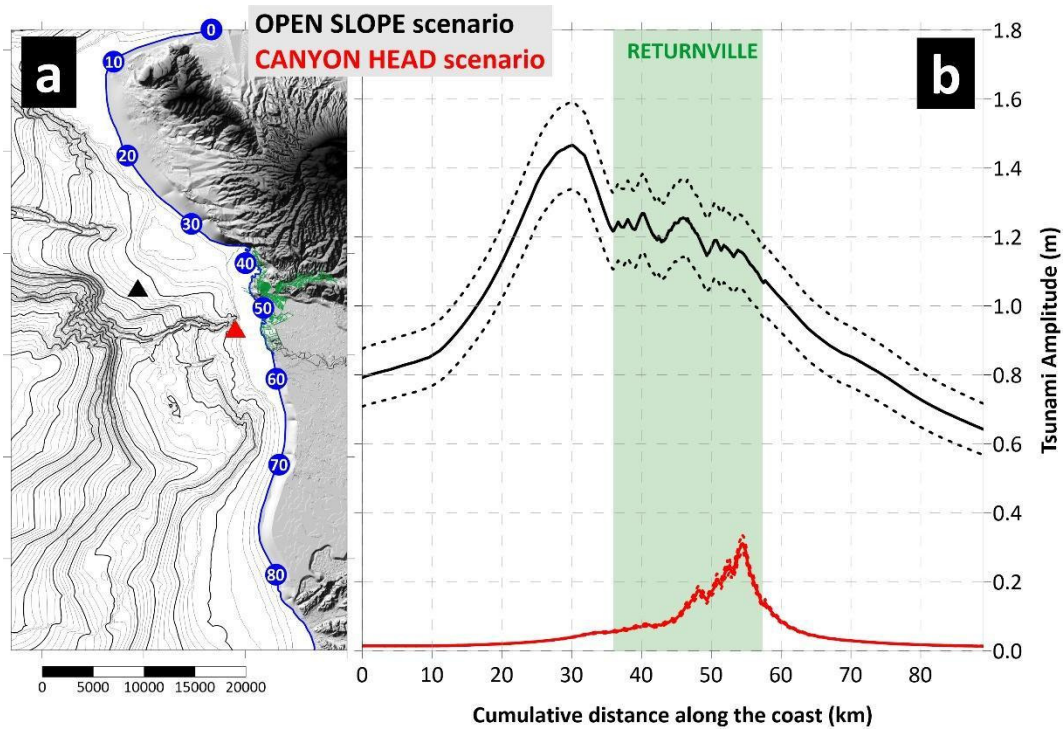

Figure 8. Panel a) map of the coastal area of the VTB with localization of the two landslide scenarios (black triangle for OS; red triangle for CH). The blue line marks the coast, with white labels in blue circles reporting the cumulative distance along the shoreline, which origin is at the northern extreme of the map. The green boundaries represent the RETURNVILLE cadastral cells, adopted to evaluate the impact of the tsunami on buildings. Panel b) Tsunami amplitude vs cumulative distance along the coast for the OS and CH scenarios (in black and red, respectively). The green-shaded area marks the position of RETURNVILLE along the coast. Dashed lines mark the uncertainties associated to the tool output.

The second phase of the tsunami hazard assessment for RETURNLAND consists of the tsunami flooding tool, which needs in input the inland topographic profile, originating from the coast, and the wave amplitude on this point: the inundation is then evaluated along this transect. A set of 1170 profiles has been generated, 100-m-spaced along the shoreline and originating from it towards the dry-land, oriented approximately perpendicular to the local coast direction, and with a longitudinal sampling of 10 m. For this case, the roughness coefficient is set to 0.030, corresponding typically to barren land. It should be noted that the results here presented do not account for the presence of buildings or other anthropogenic infrastructures, which are then neglected in this phase of the analysis.

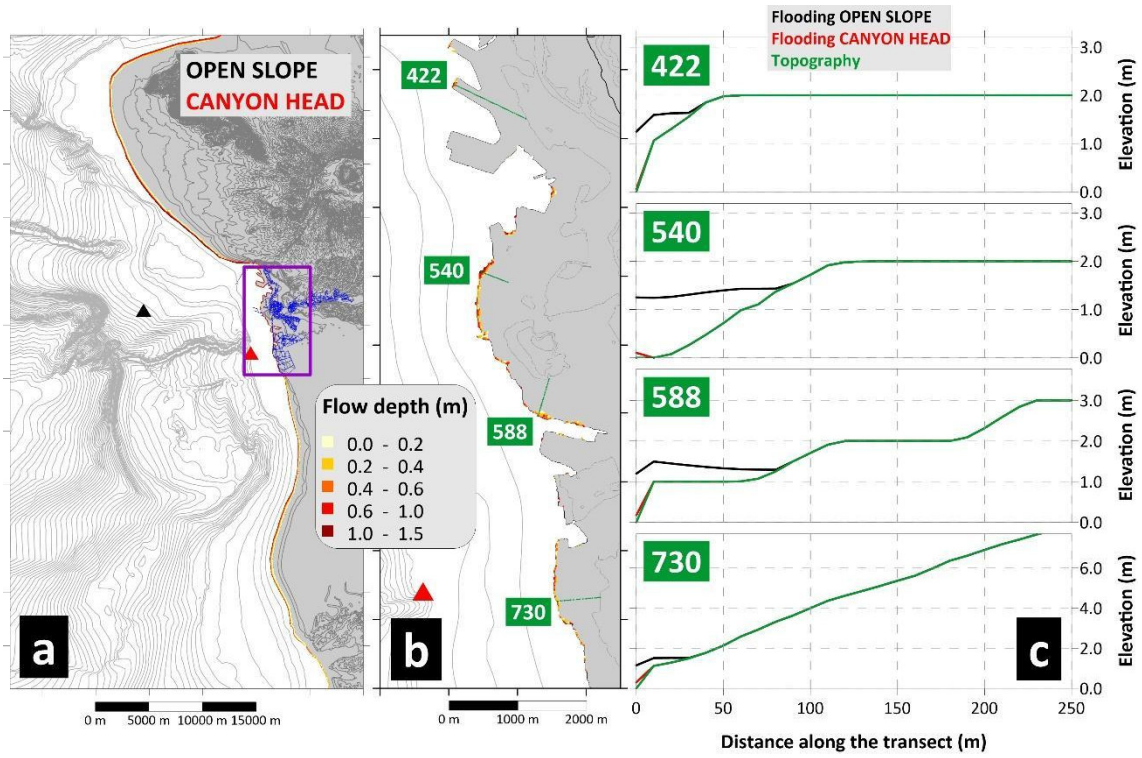

Figure 9. Panel a) map of the coastal area of the VTB with localization of the two landslide scenarios (black triangle for OS; red triangle for CH). The yellow-orange-red scale marks the flow depth for inland points affected by inundation from the OS scenario. The blue boundaries represent the RETURNVILLE cadastral cells, adopted to evaluate the impact of the tsunami on buildings. The purple rectangle evidences the area of RETURNVILLE, which is zoomed in the central panel. Panel b) Zoom on the coastal stretch of RETURNVILLE, with inundation shown by the yellow-orange-red scale. The green lines and the corresponding numerical label mark the extension of the coastal transects for which the inundation is shown in panel c. Panel c) Inundation profiles for the four transects depicted in panel b. In green the topography, in black and red the flow depth for the OS and CH cases, respectively.

The tool provides, for each transect, a profile of the flow depth along the topography: Figure 9a shows the inundation due to the OS case along the whole coastal extension of RETURNLAND, with a zoom on RETURNVILLE (Figure 9b). Here it can be noticed that the maximum inundation (yellow-red area) is limited to the first tens of meters inland. Figure 9c depicts the flow depth along some of the profiles, which extension is reported in figure 9b (in green). As expected, the OS scenario (black) produces a more extensive inundation, with water penetrating for almost 80 meters inland in certain areas (e.g., transect #540 and #588). In the first case, the flow depth exceeds 1.5 m for several tens of meters inland, indicating a potentially significant impact on population located near the shore, especially when combining this factor with flow velocity (which is not shown here). The CH scenario (in red) produces more limited flooding, consistent with the lower tsunami amplitude already described previously.

The workflow makes it possible to simulate coastal flooding triggered by a landslide that developed in a submarine environment following the generation of a tsunami wave. The resulting simulation highlights how difficult it is to predict the response of the coastal system to this type of hazard. The two landslides analyzed, which formed at different distances from the coast and in areas characterized by different geological regimes, produce different responses that are not directly linked to established principles. Therefore, these virtual analysis tools, as RETURNLAND, have now become an essential and extremely important means for multi-hazard assessment, especially for hazards originating in the marine environment, where, for many reasons, continuous monitoring of geological processes is not feasible.

4. Contribution from the VS 3 - Earthquakes and Volcanoes

The interaction of earthquakes and ground instabilities represents a primary and well studied example of multi-hazard scenario. Among the wide range of possible interactions, the simple co-occurence of earthquakes and landslides is naturally possible, but far more relevant and investigated are the scenarios with direct cascade effects (Keffer, 1984). In earthquake-induced landslides, an earthquake becomes a triggering or preparatory factor for ground instabilities, which may activate during the earthquake itself or later as a consequence of altered stability conditions. Conversely, ground instabilities can become a predisposing factor increasing the vulnerability by damaging elements at risk and thus the impact of successive earthquakes. With regard to earthquake-induced ground instabilities, even earthquakes of relatively small intensity represent a major triggering factor for landslides, debris flows, collapses, and ground fissures. Such induced ground instabilities often significantly increase or even exceed the losses caused by the earthquake itself (Azhideh et al., 2024).

The issue of earthquake induced ground instabilities has been recognized for a long time, gaining further attention with the increasing awareness of severity of losses caused by earthquake induced landslides (Del Gaudio and Wasowki, 2011). In fact, the occurrence and impact of co-seismic landslides also depends on the level of human economic development and the capability of disaster prevention and reduction. The expansion of the global economy, unplanned human activities, exploration and utilization of resources, the abuse of chemicals, the improper treatment of wastes, and associated climatic effects have enhanced the destructive power of earthquake landslides (Shao and Xu, 2022).

A high-quality inventory is an important basis for the susceptibility assessment and successive development of multi-hazard and multi-risk scenarios, (see also the pilot case below). The number and scale of the available inventories have considerably increased in the last decades. More than 130 inventories were recently reported in 2022 (Shao and Xu, 2022), even if several were not considered because of their small spatial coverage or outdated information. Criteria for generating such inventories are not standardized, and their completeness and correctness can be inadequate, which ultimately hinders the accuracy of the resulting assessments and scenarios (Pokharel et al., 2021). Beyond the direct technical aspects, the quality of the inventory and associated classification of areas and scenarios is also the basis for the administration of the social and economical resources, in both prevention and remediation.

Landslides and earthquakes are the most significant geological hazards in Italy. On the one hand, Italy is one of the most seismically active regions in Europe. Italy counted more than 20 destructive earthquakes with magnitudes of 6 or larger in the last two centuries (Prestininzi and Romeo, 2000). On the other hand, three quarters of its landscape is marked by hills and mountains, often featuring geologically weak formations and structures that are relatively prone to ground instabilities. As a result, Italy is the European country most affected by landslides, with over 635.000 landslides in the official national Italian Landslide Inventory (November 2025). More specifically to earthquake-induced landslides, the Italian Catalogue of Earthquake-Induced Ground Failures (CEDIT) reports and characterizes more than 3031 failures associated with 213 (major) earthquakes (November 2025). The catalog divides ground instabilities into ground cracks, ground changes, landslides, liquefaction, surface effects, and multiple-complex effects. Landslides account for approximately 55% of all recorded ground effects in Italy. Following the classification proposed by Keefer, 1984, approximately 40% can be classified as disrupted slides and falls, 22% as coherent slides, and 6% as lateral spreads and flows (Azhideh et al., 2024). A similar association of earthquakes and ground instabilities is also provided by the Catalogue of Strong Italian Earthquakes, which reports 1640 earthquakes with possible induced events (2337), not only related to ground instabilities (November 2025). The spatial characterization and association of ground instabilities can guide the definition or validation of multi-hazard scenarios, for example through the analysis of relative distances as a function of geological region (susceptibility) and earthquake magnitude (Salvatore et al., 2020). The spatial information regarding the ground instabilities can also guide the development and validation of toolchains for the evaluation of the landslide susceptibility, see also pilot case below.

4.1 Liquefaction

The earthquake simulation that trigger the chain of events affecting the VTB and in particular the inner Returnville is based on the strongest historical earthquake occurred in the Apennines, i.e. Mw 6.8 Irpinia earthquake of 1980. The model was developed using a Physics-Based Simulation (PBS) approach, as described

in Paolucci et al. (2026). The simulations were performed using SPEED, an open-source code based on the Spectral Element Method (SEM). This method is designed to solve elastodynamic equations in complex 3D media. The model covers a vast area of 110x147 km2, reaching a depth of 22 km. The 3D computational domain was meshed with hexahedral spectral elements, resulting in approximately 67 million spectral nodes (using a spectral degree of 4). The model achieves a deterministic frequency resolution up to 2 Hz. A 3D crustal model was implemented, including parabolic profiles for Vs and Vp in the first kilometer to represent soil property increases with depth. The simulated event is shown in Fig. 10 and was modeled as a multi-segment rupture involving three distinct fault segments activated with time delays of approximately 20 seconds each (at 0s, 20s, and 40s). Since the physical simulation is limited to 2 Hz, an Artificial Neural Network approach (ANN) was used to enrich the signals with high-frequency stochastic content, producing broad-band time histories. The model output permitted to generate Ground Acceleration (PGA) and Peak Ground Velocity (PGV) Maps. The PGA and PGV maps were generated by extracting the maximum values from the simulated horizontal velocity and acceleration time histories across the entire study area. Unlike empirical models, these maps account for the specific temporal progression of the three fault ruptures, showing how the wavefield evolves as different segments activate. Despite using a relatively "rough" modeling of local site conditions, the maps capture the realistic attenuation of ground motion with distance and the complexity caused by the multi-segment source.

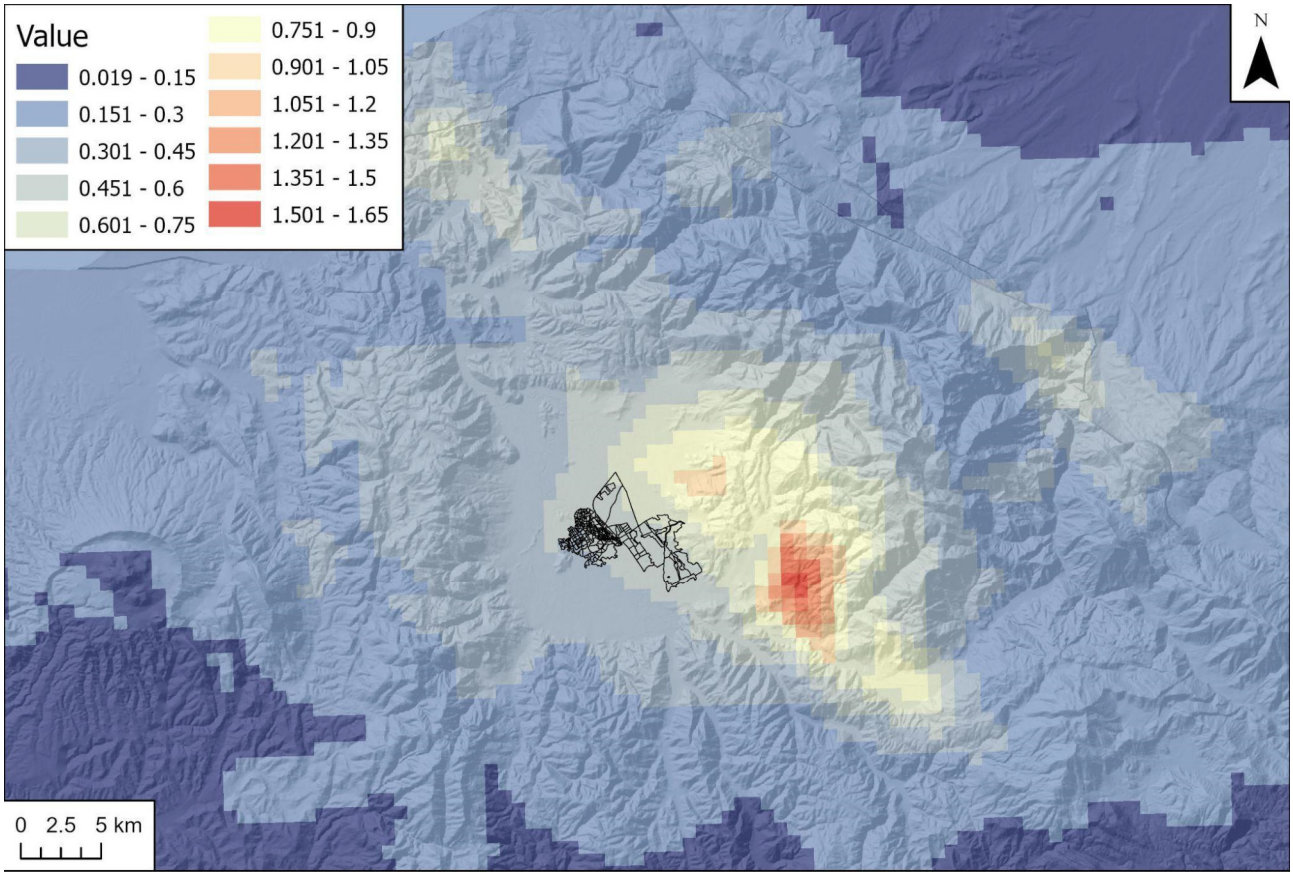

Figure 10. Distribution of the PGA at bedrock for the Apennine scenario earthquake Mw 6.8 in the VTB.

4.1.1 Liquefaction susceptibility assessment

The liquefaction susceptibility toolchain adopts the methods described in the DV 2.4.6, they are integrated in ARGUS and support multi-scale evaluation of soil liquefaction phenomenon, considering the role of predisposing, preparatory, and triggering factors. Within ARGUS, this logic underpins the entire workflow: predisposing factors represent inherent geological, geomorphological, hydrogeological and geotechnical conditions; preparatory factors encompass medium-term environmental variations that might affect the probability of occurrence; and triggering factors correspond to rapid events capable of inducing the onset of the phenomenon.

The applied liquefaction tool-chain operates on two complementary spatial scales:

- Regional scale (Level I): qualitative to semi-quantitative susceptibility assessment based on

liquefaction susceptibility classes of various types of soil deposits, following their nature and geologic age (Youd and Perkins, 1978), and Italian building code specifications (NTC, 2018). According to these latter, liquefaction is unlikely if the following conditions occur: I) maximum expected acceleration at ground level in free-field conditions less than 0.1g; II) average seasonal depth of the groundwater table higher than 15 m from ground level.

- Regional and Local scale (Level II): quantitative assessment carried out using the semi-empirical stress-based analysis. With this approach, a factor of safety FS(z) is defined for free-field conditions (i.e. without buildings and structures) as the ratio between the normalized shear stress required to induce liquefaction (CRR = cyclic resistance ratio, i.e. soil capacity) and the normalized equivalent stress induced by the design earthquake (CSR = cyclic stress ratio, i.e. seismic demand) (Boulanger and Idriss, 2014; Seed and Idriss, 1971).

The application of the liquefaction assessment toolchain within the VTB framework is designed to progressively translate geological, hydrogeological, and seismic information into a set of thematic maps that describe both the spatial distribution and the expected severity of liquefaction phenomena in the study area of the Inner Returnville. The first step in our methodology is the Level 1 Susceptibility screening. This assessment uses a decision tree based on three main factors: geology and geomorphology, the water table depth, and the Peak Ground Acceleration (PGA). For example, areas located in mountains or foothills, or those where the water table is deeper than 15 meters, are automatically classified as having 'None' susceptibility.

The geological setting was characterized starting from the lithology classes of the CARG 100k maps and updated to maximize the results of the liquefaction susceptibility assessment. The area features Holocene deposits, such as current alluvium and fluvio-lacustrine sediments, as well as older Pleistocene formations, including ancient fluvio-lacustrine deposits and alluvial fans, finally a generic rock bedrock is also identified as an area where liquefaction cannot occur, as shown in Fig. 11.

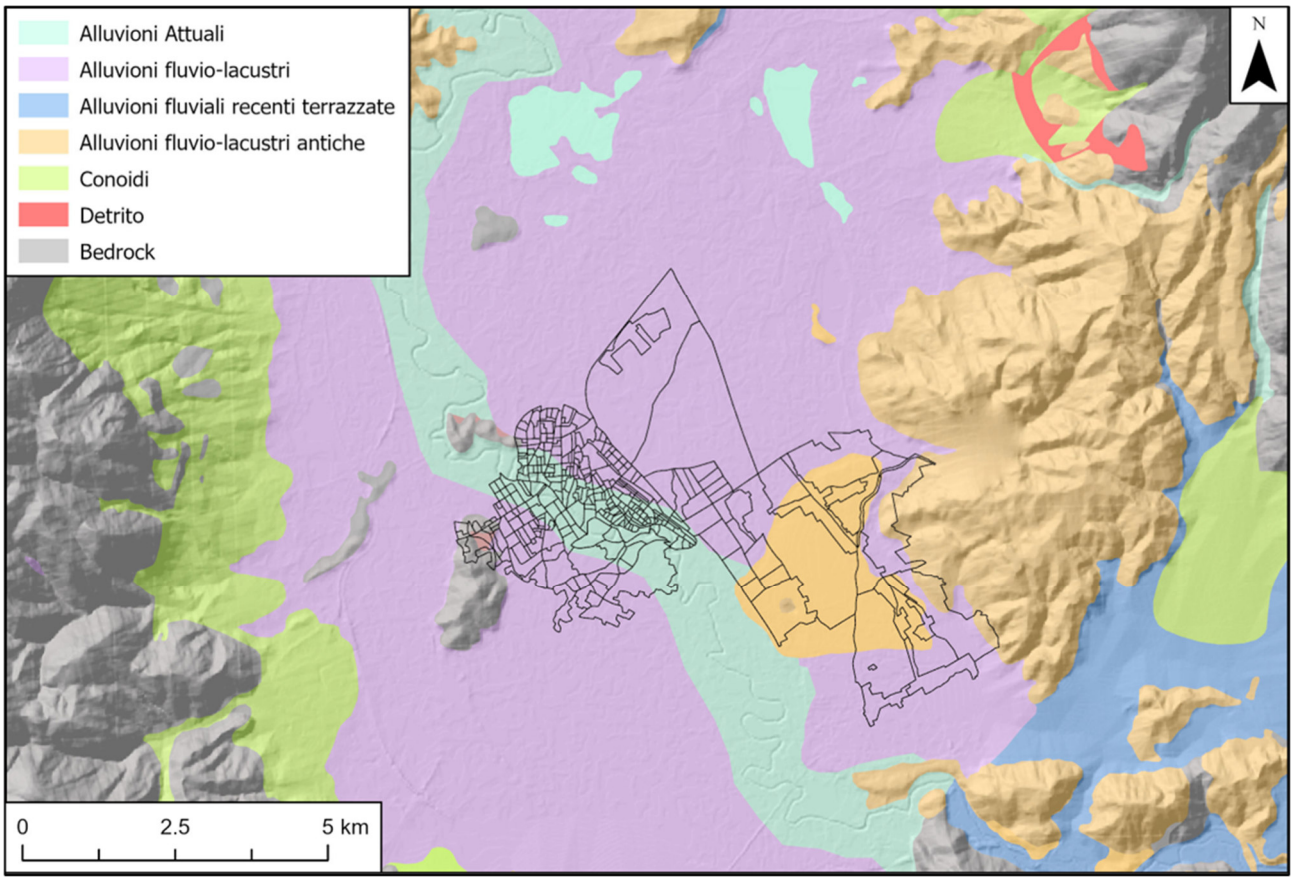

Figure 11. Geolithological setting in the neighboring of the Inner Returnville.

The hydrogeological setting is a fundamental driver for liquefaction. The water table depth was derived by subtracting the groundwater head contours from the Digital Elevation Model (DEM). This approach enabled the identification of areas with shallow groundwater conditions (depth < 15 m), which are significantly more susceptible to liquefaction triggering, as reported in Fig. 12.

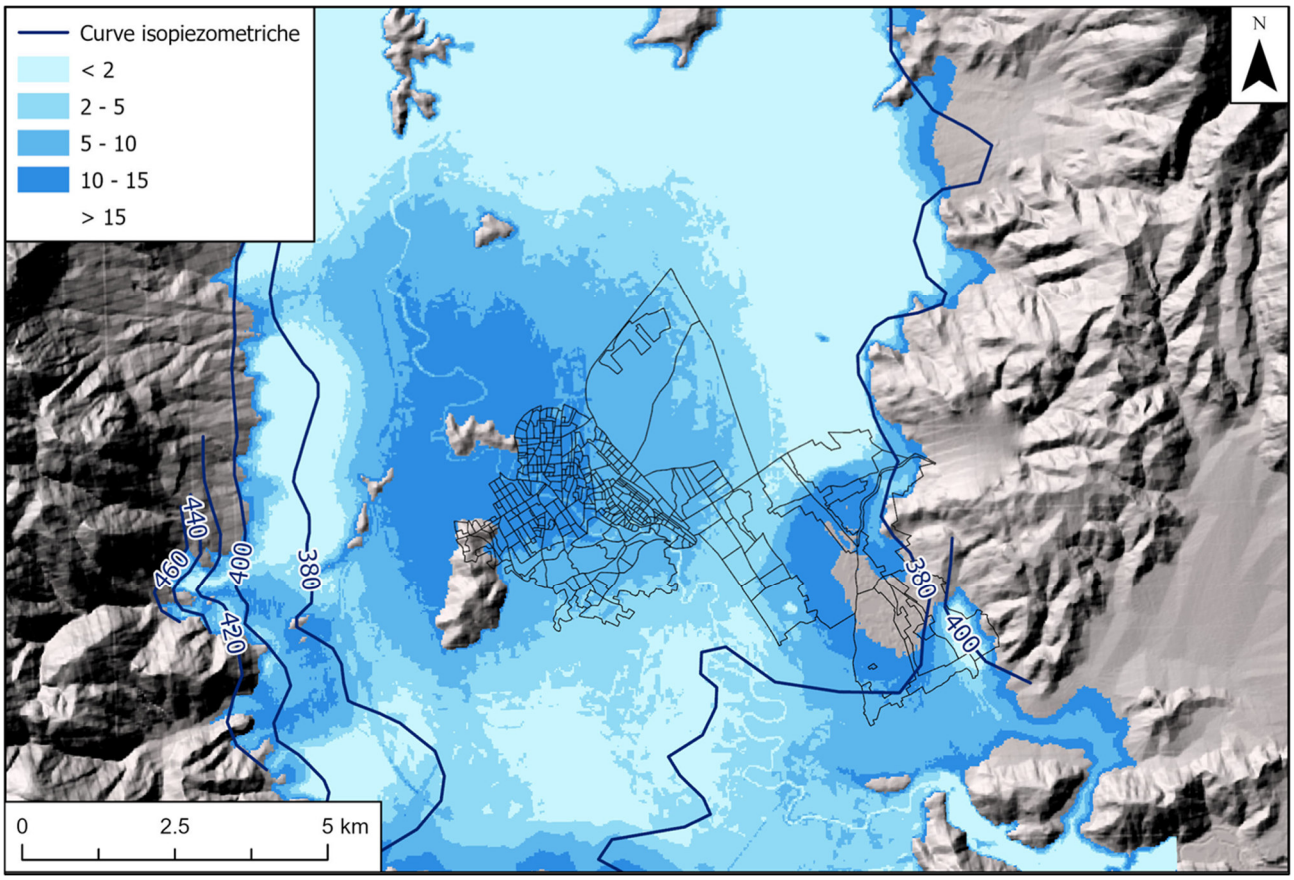

Figure 12. Hydrogeological map of the plain area of the Inner Returnville

The seismic scenario map, expressed in terms of peak ground acceleration (PGA), represents the triggering factor of the process and allows the differentiation of areas subjected to low, moderate, or relatively high seismic demand. The combination of these three components—geology/geomorphology, groundwater table depth, and PGA—leads to the construction of the Level I liquefaction susceptibility map. To evaluate the seismic demand, we took the seismic scenario in terms of PGA distribution provided for the VTB simulating an Apennine earthquake. By integrating the geological, hydrogeological, and seismic data, we produced this Level 1 Susceptibility map shown in Fig. 6. This provides a first-order identification of the zones where liquefaction risk is potentially significant and requires further investigation.

The Level I susceptibility map clearly distinguishes areas with no expected liquefaction susceptibility, typically corresponding to mountainous, foothill, or hilly sectors, zones with deep groundwater conditions, or areas characterized by very low seismic input. Conversely, extensive portions of the flat alluvial plain emerge as potentially susceptible, with susceptibility levels ranging from medium to very high as shown in Fig. 13.

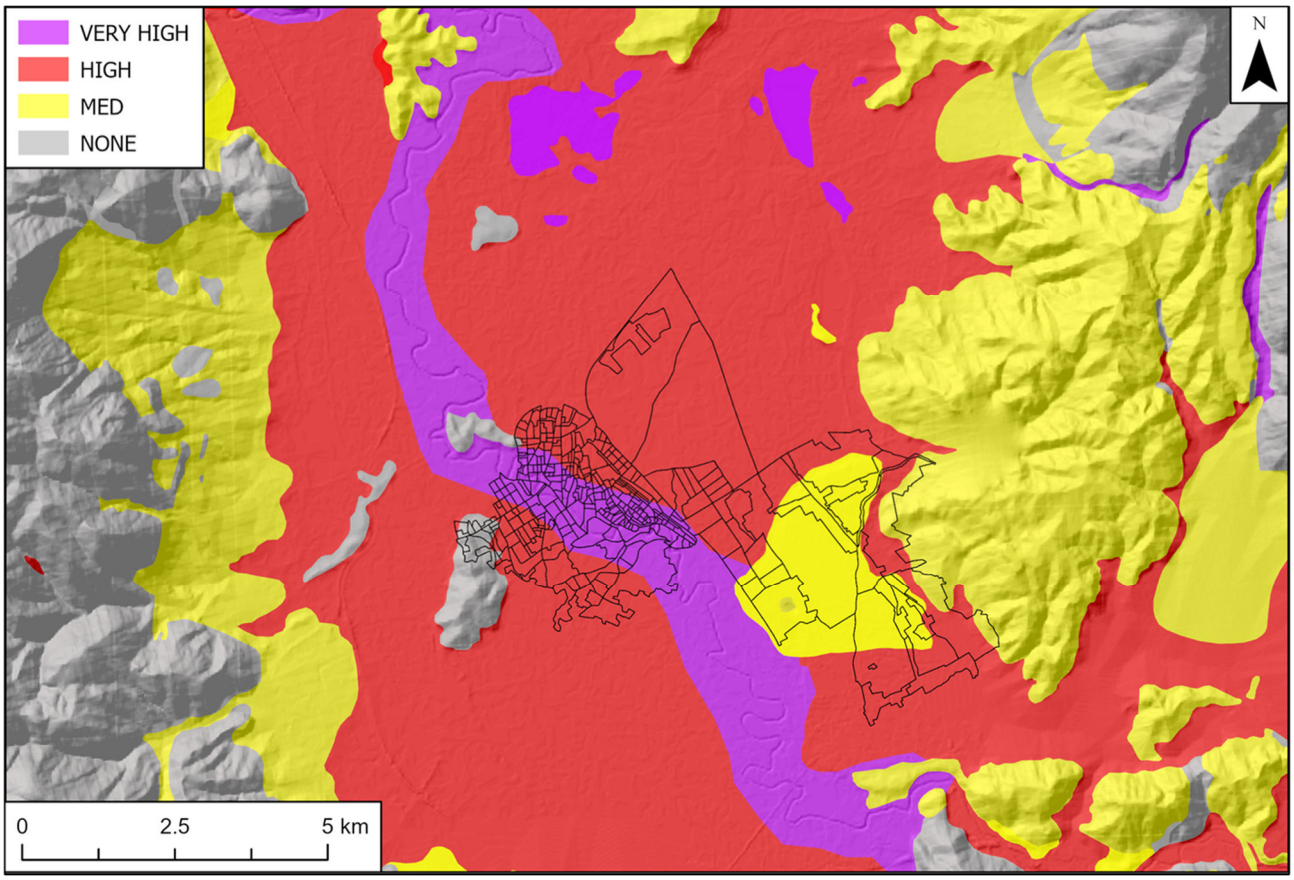

Figure 13. Level I liquefaction susceptibility map of the plain area of Inner RETURNVILLE.

This first susceptibility map plays a key role in guiding the transition to the Level II analysis, by identifying those sectors where a more detailed, quantitative assessment is required. In this further step, a regular grid was set around the Inner RETURNVILLE, with 500x500 m cells, each one hosting 1 CPT, for a total of 457. The investigation depths vary between 20 and 40 m, which allow a site-specific evaluation of soil resistance to liquefaction (See Fig. 14a).

To ensure a realistic representation of seismic loading at the ground surface, the analysis incorporates a stratigraphic amplification map derived following the methodology by Tropeano et al. (2018), after assigning a seismic soil class for each lithology. This step allows the conversion of PGA at bedrock into surface PGA (PGAs), which directly influence the Liquefaction potential calculation. The amplification map highlights the role of local soil conditions in modifying the seismic demand, particularly in sectors characterized by soft, unconsolidated sediments, also accounting for non-linear effects due to high Magnitude earthquakes, as reported in Fig. 14b.

Using these data, the Index of Liquefaction Potential (IL) is computed for each grid cell following the method proposed by Iwasaki et al. (1982) and summarized in DV 2.4.6. The resulting IL map provides a quantitative representation of liquefaction severity, accounting not only for the presence of liquefiable layers but also for their depth distribution through a weighting function. Spatially, the IL map reveals significant variability within the areas previously classified as susceptible at Level I. Zones with moderate IL values are interspersed with areas exhibiting very high IL values, indicating a strong spatial heterogeneity of liquefaction potential even within similar geological settings. This analysis was carried out considering two variations of preparatory conditions, i.e. the groundwater depth. In Fig. 15a, the hydrogeological setting represented in Fig. 12 is used, it shows areas where the phenomenon is unlikely to occur due to a deeper groundwater table. On the contrary, Fig. 15b is obtained assuming a Climate Change scenario, where the groundwater table is shallower and located at 1.5 m from ground level. In this map, the whole susceptibility is higher and the only areas where no susceptibility is reported is that where bedrock crops out.

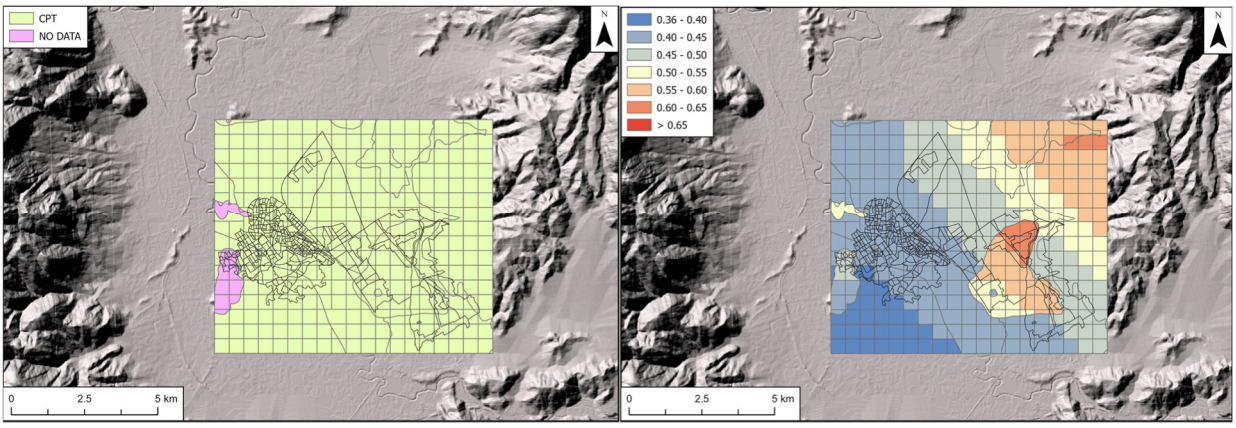

Figure 14. A) Grid 500x500 m representative of CPT distribution (green cells). B) Distribution of amplified PGAs at surface.

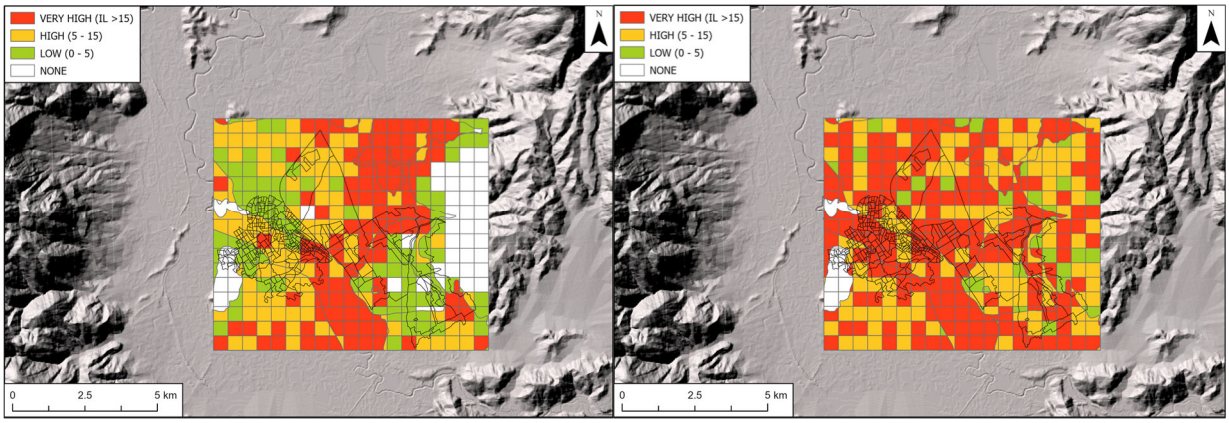

Figure 15. A) Level II liquefaction susceptibility map for the hydrogeological setting reported in Fig. 12. B) Level II susceptibility map for a shallower groundwater table at 1.5 m from ground level.

Building on the IL results, the analysis further advances toward impact-oriented outputs by estimating liquefaction-induced vertical settlements under free-field conditions (see Figs. 16a and 16b). The settlement map is obtained by integrating the vertical strain of individual liquefiable layers, following the formulations proposed by Zhang et al. (2002). For a representative groundwater table depth of approximately 1.5 m, the results show expected settlements ranging from a few decimeters to more than half a meter in the most critical areas. These values clearly indicate that liquefaction effects may result in significant ground deformation, with potentially severe consequences for structures and infrastructure.

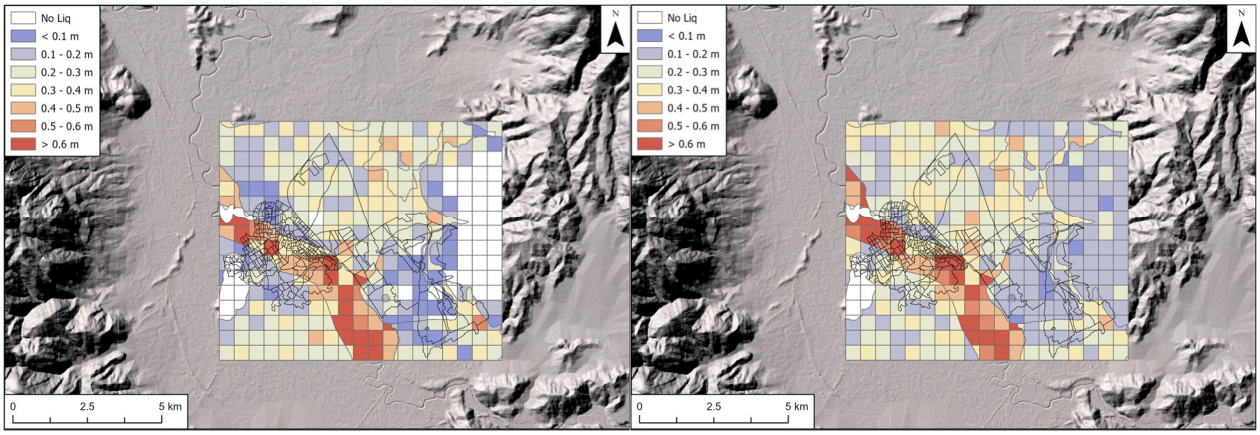

Figure 16. A) Liquefaction-induced settlements for the hydrogeological setting reported in Fig. 12. B) Liquefaction-induced settlements for a shallower groundwater table at 1.5 m from ground level.

Overall, the sequence of maps produced through this toolchain—from geological and hydrogeological framing, through Level I and Level II susceptibility, to IL, settlement, and expected damage—provides a coherent and

progressively refined representation of the liquefaction impact chain in the VTB area. This integrated mapping approach supports a clear understanding of where liquefaction is likely to occur, how severe its effects may be, and which areas should be prioritized for risk mitigation and resilience planning within the RETURN Digital Ecostystem.

4.2 Contributions from VS3

The vertical spoke 3 Earthquakes and Volcanoes covered several aspects that are relevant to the above multi-hazard scenarios. With regard to earthquakes, the focus of the work packages 4, 5, 6, and 7 ranged from engineering aspects (e.g., monitoring, early warning, and rapid response) to more conceptual and general aspects of risk metrics and maps in a resilience-oriented and climate-proof perspective.

The WP 4, focused on reviewing and advancing novel solutions for real-time monitoring. In fact, real-time monitoring of earthquakes enables the rapid detection of seismic activity and supports early-warning systems. As for the weather monitoring, the earthquake early warning systems, in turn, can interact with site-specific monitoring and warning systems for ground instabilities. The WP 4 reviewed how today's monitoring networks combine ground sensors, GPS data, and fast data-processing algorithms to deliver alerts within seconds, and many regions now integrate these warnings into public safety systems and critical infrastructure. Italy, as other developed countries, has a structured monitoring system based on a high-density network. The system is managed by INGV, Department of Civil Protection, and National Institute of Oceanography and Applied Geophysics (Margheriti et al., 2021; Picozzi et al., 2015).

The INGV system follows a combined-incremental surveillance solution for the detection and characterization (position, intensity) of new earthquakes. At first, an automatic detection and localization is performed to trigger a sequence of communications and warnings to the relevant organizations, but also to the general public. Successively, more information is collected and more precise analyses and validations are performed and made public. Information regarding earthquake-induced ground deformation becomes available a few hours after the earthquake event, from GPS data or synthetic aperture radar interferometry analysis. Tasks 3.4.1 and 3.4.2 from the VS3 reviewed and investigated solutions for early warning and rapid response for earthquakes. The resulting contributions from their tasks highlights the increasing number of technical solutions and variety of algorithms proposed and implemented. In particular, they focused on the increasing use and integration of physical models and artificial intelligence. The methodological advances are deemed relevant for the simulation of multi-hazard scenarios of ground instabilities at different scales.

Directly, the improvements in the early warning system would contribute to capacity-response and thus reduce the vulnerability-risk: an earthquake warning from a regional/national monitoring system triggers a predefined set of responses and warnings associated with an increased ground instability hazard at the local scale, possibly taking advantage of local-existing communication services. Here, it is important to highlight two possible advantages with respect to the single-hazard earthquake scenarios. First, it has been documented and discussed how even relatively small accelerations can trigger landslides and other ground instabilities (Azhideh et al., 2024). A regional/national early warning could prove relevant even in moderately or lightly shaken areas, at larger distance from the earthquake epicenter, whose leading times (time available for the response) are larger and allow more effective responses. This is in contrast with "pure" earthquake scenarios, particularly for inland and shallow earthquakes, whose blind zones (i.e, no leading time) covers a large part of the significantly impacted areas, challenging and hindering the benefits of existing early warning systems (Wald, 2020). Second, additional leading time is expected from the multi-hazard cascade of events. While this would naturally depend on the type of the ground instability and its position relative to the exposed elements, such "secondary" leading time would be associated with an actual deformation or transport process and thus likely match or exceed the otherwise available leading time due to the fast seismic propagation.

Indirectly, the increasing quality and extent of exiting inventories on earthquakes, with associated propagation scenarios and induced ground instabilities, provide valuable information on the expected site acceleration and landslide magnitude–distance scenarios (Bragato et al., 2021; Margheriti et al., 2021; Salvatore et al., 2020). Such information can combine with the site hydro-geotechnical characterization (e.g., critical acceleration) to provide maps that classify sites based on their potential for triggering earthquake-induced ground instabilities (Azhideh et al., 2024). Two main approaches exist to preemptively estimate earthquake-triggered effects on ground instabilities: a physical approach in which the expected earthquake-induced accelerations are included in the stability analysis (e.g., Newmark's method); and a statistical one which can take advantage of the

increasing quality of the earthquake-induced landslides, such as the Italian CEDIT (Amato et al., 2023; Salvatore et al. 2020). Finally, the methodological advances on the early detection of possible earthquakes could be transferred to the early warning technologies, which often include accelerometers and geophones (Pecoraro, 2019).

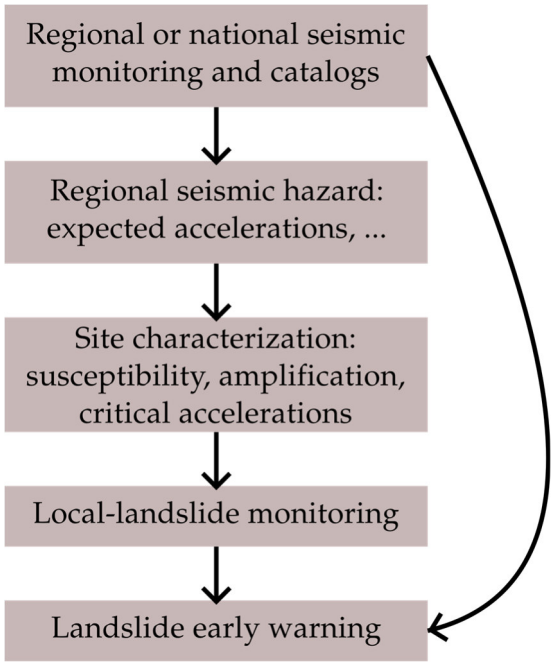

Figure 17. Synergy between a national/regional earthquake monitoring system, as resulting inventories, and local early warning systems that monitored a specific landslide.

The task 3.4.4 focused on early-warning delivery platforms and decision modules that would activate in case of earthquake events. All the reviewed and investigated solutions are very promising for earthquake-induced multi-hazard scenarios, being earthquake tragically capable of causing not only ground instabilities, but also floods, fires, and other human-specific emergencies (power plants and energy networks-pipelines, infrastructures, and key elements such as medical and resources). On the one hand, as briefly described above, these solutions could interface with existing monitoring systems of ground instabilities, which could be triggered or set in a pre-alert state, depending on the site-specific conditions. On the other hand, the end-to-end solution could be resealed and adopted by the local early warning systems, based on the significant overlap in terms of technological and theoretical challenges (Pecoraro et al., 2019; Piciullo et al., 2020). For example, Acampora et al., 2025, proposed the use of fuzzy rule-based architectures for the design of a rapid response system that can monitor the condition and of the affected areas/buildings and peoples therein and thus provide emergency priorities. Here, the adopted fuzzy rule-based accounts for the uncertainties in impact scenarios, where sets of general rules can be defined but the available information (prior or during the emergency) may not support traditional - "exact" approaches. This technological solution could contribute to multi-hazard scenarios of ground instabilities as comparable impact on building and people may be expected.

Moving from the monitoring and early warning systems to the impact scenarios, the work packages 5 and 6 covered the analysis of impact on the built environments and the investigation of sustainable solutions that could reduce their vulnerability. The tasks 3.5.2 investigated novel solutions for modeling the propagation and damaging effects of seismic waves, paying particular attention to the unique characteristics of urban environments and associated multi-hazard urban scenarios. Di Trapani et al., 2024, task 3.6.2, investigated novel solutions for the health monitoring of masonry structures and infrastructures. The authors focused on the use of piezoresistive and capacitive technologies, low-cost and robust solutions that could complement existing technologies (e.g., Micro Electro-Mechanical Systems and smart bricks). In the frame of multi-hazard scenarios, the improved real-time monitoring of structural health and stress can contribute to the existing early warning systems and/or guide more effective responses, for example by informing on the extent of the induced damages and possible successive hazards. Finally, the development of new technologies in more controlled conditions (e.g., buildings) could pave the way to a technological transfer towards natural systems in general and ground instabilities specifically.

Other tasks of the WP 6 aimed at multi-vulnerability scenarios and associated analysis of the expected impact. These activities adopted the SNOWBALL approach, initially published by Zuccaro et al., one of the WP leaders (Zuccaro et al., 2018). The approach provides a frame-work for describing multi-hazard cascades integrating:

1) identification of the scenario spatial and temporal windows,

2) identification of triggering-primary hazards and secondary hazards

3) selection of the cascading processes,

4) modelling and analysis of the cascading effects, based on a probabilistic definition of the triggering-initial hazards

5) dynamic evaluation of the vulnerability within each scenarios, i.e., accounting for the temporal variability of the vulnerability through the scenarios triggered by initial hazards of different magnitudes

6) spatial and temporal loss estimation within the initially defined model domain.

Of specific interest for this task, the SNOWBALL framework distinguishes both primary and secondary ground instabilities, as well as different types of ground instabilities. Primary instabilities function as triggering hazards, e.g., a landslide triggering a cascade of events, while secondary instabilities are induced by earthquakes, volcanoes, or extreme weather events. Ground instabilities are divided in landslides/lahar, ground collapses, soil subsidence, and ground heave. At its core, the framework defines a matrix describing both the probability of interaction between hazards within the cascade and the actual compatibility of the hazards within model time and space windows. For example, an earthquake would trigger ground instability depending on their interaction level at the simulated magnitude, but also accounting for the compatibility-probability of occurrence of such landslides. Hence, as the definition of interaction and compatibility is a fundamental step, valuable synergy exists between advancing the SNOWBALL model and above reviewed databases of earthquakes and earthquake-induced ground instabilities (CEDIT - https://gdb.ceri.uniroma1.it/index.php/view/map/?repository=cedit&project=Cedit). Possible contributions may also result from the integration of the SNOWBALL framework and model for the calculation of the instability susceptibility, the latter being able to provide the needed “compatibility” map required in SNOWBALL. As an example, see the application of the R.Slope.Stability model to the pilot case of Stigliano, presented below.

4.2.3 Simulation tools in the volcanic area of the VTB

Volcanic eruptions can produce a wide range of hazardous phenomena, including tephra deposition and pyroclastic density currents (PDCs). The severity of their impacts depends on eruption magnitude and distance from the volcanic vent. When critical thresholds are exceeded, tephra accumulation and the dynamic pressure of PDCs may cause significant damage to buildings and infrastructure. To assess these potential effects, advanced numerical modeling techniques were applied to the RETURNVILLE area.

The evaluation of explosive eruption hazards in RETURNVILLE focuses on two major processes: tephra fallout and pyroclastic density currents. Although these phenomena originate from different eruptive mechanisms, both represent serious threats to infrastructure, the environment, and exposed populations.

4.2.4 Tephra fallout

To assess the potential impact of tephra fallout, a representative output of ground tephra load (kg/m²) was selected from a large set of numerical simulations presented in Massaro et al. (2023). That study provides a long-term assessment of tephra fallout hazard in southern Italy associated with the three active Neapolitan volcanic systems: Somma–Vesuvius, Campi Flegrei, and Ischia. The simulations were performed using the Eulerian tephra dispersion model FALL3D-8.0 (Folch et al., 2020), which solves the advection–diffusion–sedimentation (ADS) equations to simulate the transport and deposition of volcanic tephra. The model allows for a wide range of parameterizations, including eruptive source characteristics, ash aggregation processes, spatial discretization, and the gravitational spreading of the umbrella cloud (Costa et al., 2013).

Meteorological conditions were derived from the fifth-generation ECMWF global reanalysis dataset (ERA5; Hersbach et al., 2020), with a spatial resolution of 0.03° × 0.03° and a temporal resolution of 3 hours. Volcanic scenarios were generated through random sampling of eruptive source parameters representative of the medium-to-high eruption class of Campi Flegrei, as defined in previous studies (Sandri et al., 2016; Montesinos et al., 2022; Massaro et al., 2023).

The simulation output shown in Figure 18 was spatially translated to the Returnville volcanic vent (red point) and represents an eruption size consistent with the medium-to-high magnitude class defined for Campi Flegrei (e.g., Agnano–Monte Spina eruption; de Vita et al., 1999). In this scenario, the main dispersal axis extends across the inland area of Returnville, resulting in potential tephra loads of up to approximately 600 kg/m². This value corresponds to an estimated deposit thickness of about 60 cm, assuming an average deposit density of 1000 kg/m³.

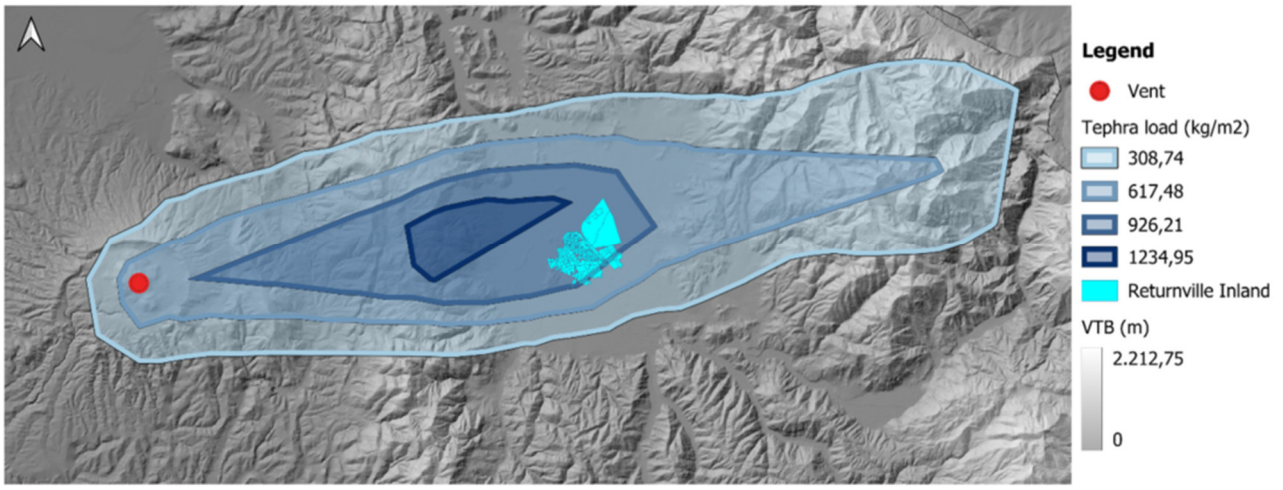

Figure 18. Simulated tephra load (kg/m²) generated using the FALL3D-8.0 model. The red dot marks the location of the eruptive vent, while the cyan area indicates the Inland Returnville zone. The background represents the topography (VTB, in meters).

4.2.5 Pyroclastic density currents (PDC)

PDCs are fast-moving and highly destructive flows typically associated with medium- to large-magnitude explosive eruptions (Dellino et al., 2019). They can be generated by several eruptive processes, including column collapse, lava dome failure, directed blasts, phreatic and phreatomagmatic explosions, and caldera collapse (Lube et al., 2020). PDCs may travel several kilometers from the vent, causing severe damage to infrastructure and posing serious risks to exposed populations (Dellino et al., 2021).

The hazardous nature of PDCs is primarily related to their high velocity, temperature, mobility, and dynamic pressure, which can result in structural failure of buildings and lethal conditions due to hot, fine ash. A detailed understanding of PDC generation, propagation, and interaction with the built environment is therefore essential for reliable risk assessments. Evaluating PDC impacts against known resistance thresholds of building elements (e.g., walls, doors, and windows) supports the development of effective mitigation strategies (Doronzo and Dellino, 2011).

For these reasons, the second application of the VTB in a volcanic context focuses on PDCs generated by eruptive column collapse and simulated over real topography. The modeled scenario includes the Returnville dock area, located approximately 11 km from the volcanic vent, a distance comparable to that of Pompeii during the 79 AD eruption of Mount Vesuvius. Numerical simulations were performed using the ANSYS Fluent modeling framework. ANSYS Fluent is a widely adopted multiphase Computational Fluid Dynamics (CFD) software that supports different modeling approaches for multiphase flows, including the Discrete Element Method and the Two-Fluid Model (TFM). For the selected scenario, TFM was adopted as it is particularly suited to flows involving large particle concentrations, such as pyroclastic density currents (PDCs) (Neglia et al., 2023).

The computational domain is a rectangular volume measuring 20 km × 6 km × 7 km along the x (flow direction), y, and z axes, respectively. It is discretized using a body-fitted, unstructured hexcore mesh composed of approximately one million cells. Mesh refinement was applied at the vent and column-collapse region, along the main flow path, and around the dock area located 11 km from the vent. Cell sizes in the refined regions are set to 50 m, with further refinement to 10 m in the dock area to accurately resolve flow dynamics and associated dynamic pressures. The flow inlet is located at the volcano summit within the caldera (Fig. 19a). The mass eruption rate at the inlet is set to 1.6×10^8 kg s^{-1}, a value within the range (10^7–10^9 kg s^{-1}) typically associated with the generation of PDCs (Cioni et al., 2000). The solid phase at the inlet is characterized by a density of 1550 kg m^{-3}, a particle diameter of 25 μm, and a temperature of 800 °C.

Figure 19 illustrates the velocity magnitude of pyroclastic density currents (PDCs) generated by column collapse over the reconstructed topography, together with the vertical profile of dynamic pressure in the dock area.

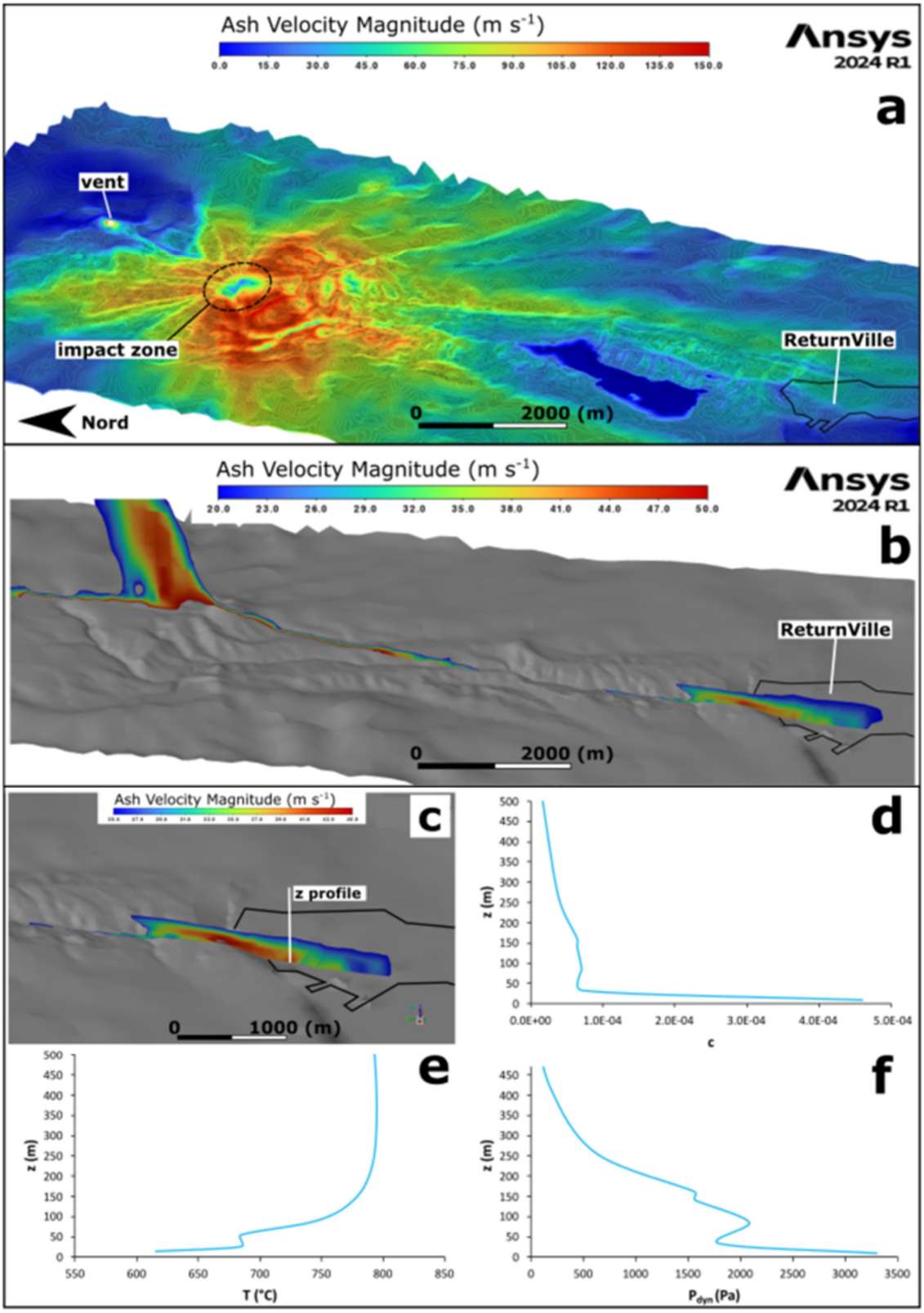

Figure 19. a) Contour map of ash velocity magnitude at ground level, b) ash velocity magnitude along a vertical yz-slice, c) zoomed view of ash velocity contour in the RETURNVILLE area, vertical profile of (d) ash concentration, (e) temperature, and (f) dynamic pressure in the inundated area.

After impacting the ground (dashed line in Fig. 19a), the PDCs spread radially and propagate toward the domain boundaries, preferentially following the main ravines. The impact zone is characterized by low velocities, associated with granular compaction and a localized increase in gas pressure that promotes lateral expansion of the flow. Maximum velocities of approximately 150 m s^{-1} are reached immediately downstream of the impact area, where the currents overtop local topographic highs before becoming channelized within the main ravines, with velocities of 70–100 m s^{-1}. In the vicinity of the RETURNVILLE area (highlighted in Fig. 19a), flow velocities decrease to 40–50 m s^{-1}. A yz-plane slice of ash velocity (Fig. 19b) shows the portion of

the flow impacting RETURNVILLE, with an estimated thickness of about 200 m and peak velocities of 52 m s^{-1}. A secondary pulse follows the main flow, contributing to the overall hazard. A close-up of the dock area (Fig. 19c) highlights the flow passage over a concave-downward slope near RETURNVILLE, where a hydraulic jump occurs, resulting in reduced velocities and increased flow thickness as the regime transitions from supercritical to subcritical conditions. Figures 19d–f show the vertical profiles of dynamic pressure (P_dyn), temperature (T), and solid concentration (c) in the same area. Despite traveling approximately 11 km from the vent across complex terrain, the PDC maintains dynamic pressures of about 3.3 kPa at 10 m above ground level, with solid concentrations of ~5×10^{-4} and temperatures around 600 °C. These values are consistent with previous studies (Baxter et al., 1998; Dellino et al., 2008; Valentine, 1998) and indicate the potential for damage to building openings, facilitating the ingress of hot ash into structures. In this scenario, thermal effects and ash concentration represent the dominant hazards, exceeding the mechanical impact on buildings, especially given the prolonged exposure time of several minutes during flow passage.

5. R.Slope.Stability applied to the Stigliano demonstration case

A set of demonstration cases were identified within the study activities of the WP 5 to test the operational toolchains that were developed or selected by the VS 2 for the assessment of ground instabilities. DV 2.4.4 provides an in-depth description and analysis of these toolchains; hence, this section focuses specifically on the application of the stability model *r.stability.slope* (version 2.0) to the demonstration case of Stigliano.

The Stigliano site is a hilly area of 15 km² surrounding the small town of Stigliano, in the Matera province, Basilicata region. The site was recognized by the River Basin District of the southern Apennines (ABDAM) as an area characterized by widespread earthflow and other landslide phenomena, affecting flyschoid deposits (Guerricchio et al., 1992; Vicari et al., 2019). The site geologic formations include the 'Varicoloured Clays' of Cretaceus-Eocene age, the 'Stigliano Formation' (or Numidian Flysch), the 'Serra Cortina Marls' and the 'Serra Palazzo Formation', all of Aquitanian-Helvetian age, the Calcarenites and Subapenninic Marly-blu Clays of the Plio-Pleistocene age. Guerricchio et al., 1992, provide a good description of the geological setting predisposing factors for the ground instabilities. In October 2024, a group from the RETURN project visited the site to update and validate the information reported in literature and in the hydro-geomorphological setting plan (ABDAM, 2018). Additional landslides were indeed mapped during the field work; these landslides were successively used to validate the susceptibility map obtained from the numerical models.

The stability model r.slope.stability was chosen because it is designed for roto-translational landslides, with slip surfaces of ellipsoidal shape, which were deemed to sufficiently describe the landslide - earthflow occurring at the Stigliano site. In addition, the model can also account for seismic-induced instabilities by using a pseudostatic or Newmark approach, which positively aligns with the focus on multi-hazard scenarios. Finally, the r.slope.stability model has been developed and maintained with the contribution of Italian authors who also contributed to its application in the frame of RETURN pilot cases.

R.slope.stability V2.0 is designed for physically-based slope stability analyses over large areas (up to hundreds of square kilometres). It offers five modes of physically-based slope stability simulations. Four of them build on large numbers of randomly located, randomly sized slip surfaces, whereas one employs the infinite slope stability model. In principle, r.slope.stability uses an elevation raster map and a system of soil classes and layers. Each soil class or layer is associated with geometric and geotechnical characteristics. While it is possible to test only ellipsoids with fixed parameters, i.e., adopting a deterministic definition of slip surfaces, here we took advantage of the probabilistic generation/evaluation within given ranges of length, width, and depth (Mergili et al., 2014a,b). The probabilistic approach was ultimately chosen because of the early stage of the Stigliano pilot case, with regard to limited knowledge of the soil classes and geometries of the slip surfaces. For the probabilistically defined-evaluated surfaces, the model applies a limit equilibrium approach with a Mohr-Coulomb failure criterion. Relevant to the multi-hazard scenarios, the model also distinguishes different levels of water contents, producing susceptibility maps for dry or saturated soil. As for the geothechnical characteristics, saturation is assigned to the model through the soil classes.

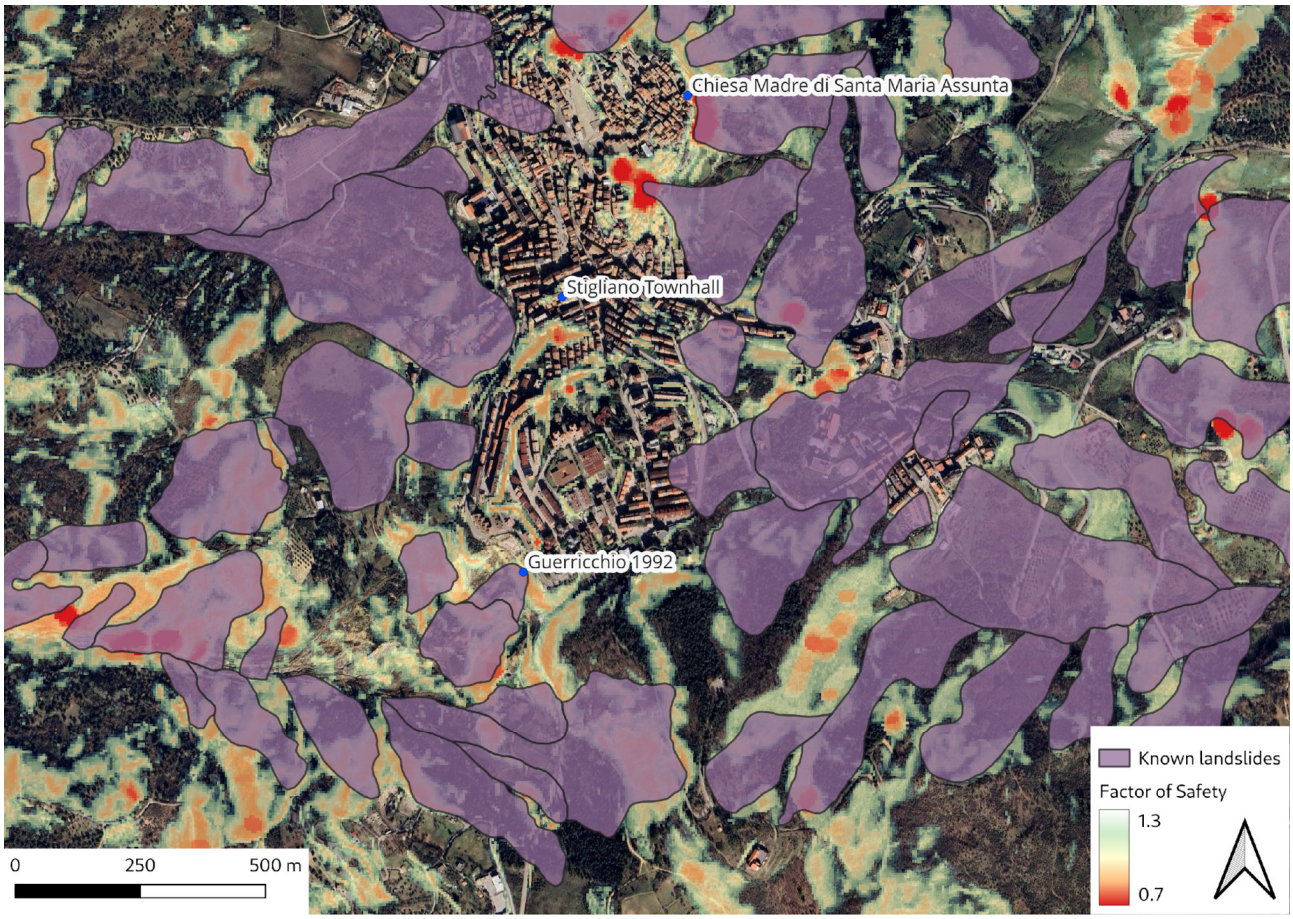

Figure 20. Known landslides and calculated factor of safety for the area surrounding Stigliano. Only the roto-translational landslides are included to better match the model outputs. Reported landslides were identified or confirmed during the field campaign in October 2024. Note that the model output is continuous and covers the entire area but higher transparency given to the factor of safety above 1.2 to ease visualization.

Figure 20 shows the susceptibility map calculated by r.slope.stability for the areas around the town of Stigliano, where several slopes prone to instability were correctly recognized. Regions with a factor of safety lower than 0.8 match existing and well documented active landslides. For example, the landslide described by Guerricchio et al., 1992 in the south west part of the town. Similarly, at north east, the two main landslides still impacting the town are recognized and very low factors of safety values are calculated in correspondence of their crowns. This first model was parameterized considering slip surfaces with a maximum length of 50 m and a maximum width of 40 m. While water content conditions were assigned homogeneously to the layers, and independently from actual weather scenarios, future applications could chain the TOP model and this stability model. The resulting toolchain would take expected rainfall events and calculate the corresponding mm of infiltration and thus water condition of the subsurface layers used in the successive stability computation.

Figures 21 and 22 show the susceptibility map in an area located southwest of Stigliano, where landslides are expected because of the similar geology but they were not mapped during the field campaign. Hence, the two figures offer the possibility to further test the model and take advantage of satellite images. As visible, the factor of safety assumes values of significantly below 1 in the slopes that appear actively or recently impacted by landslides. Beyond the model validation itself, the positive comparison encourages future numerical evaluations on a wider area and could guide future field campaigns.

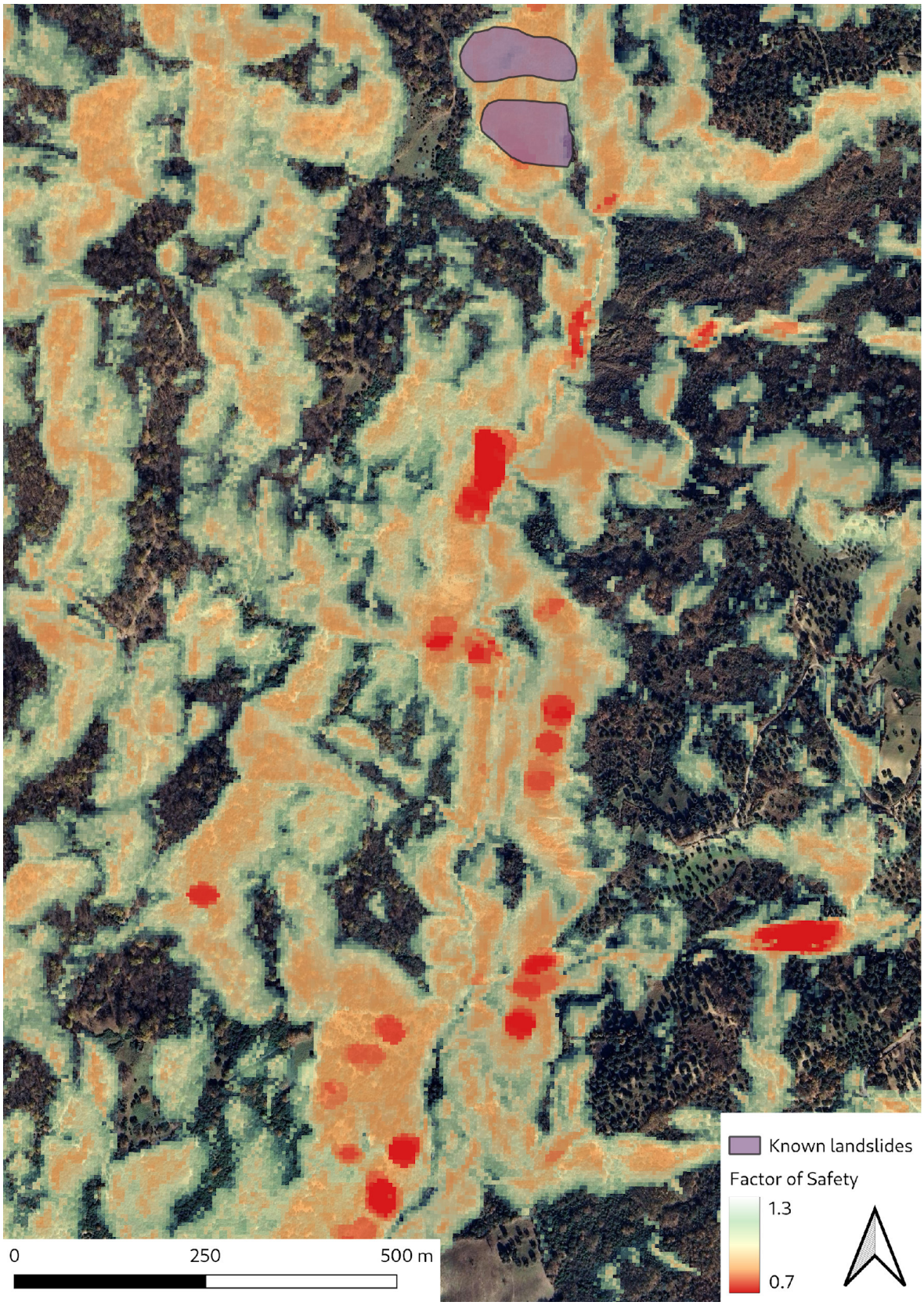

Figure 21. Factor of safety calculated for the area southwest of Stigliano, which was not mapped during the field campaign.

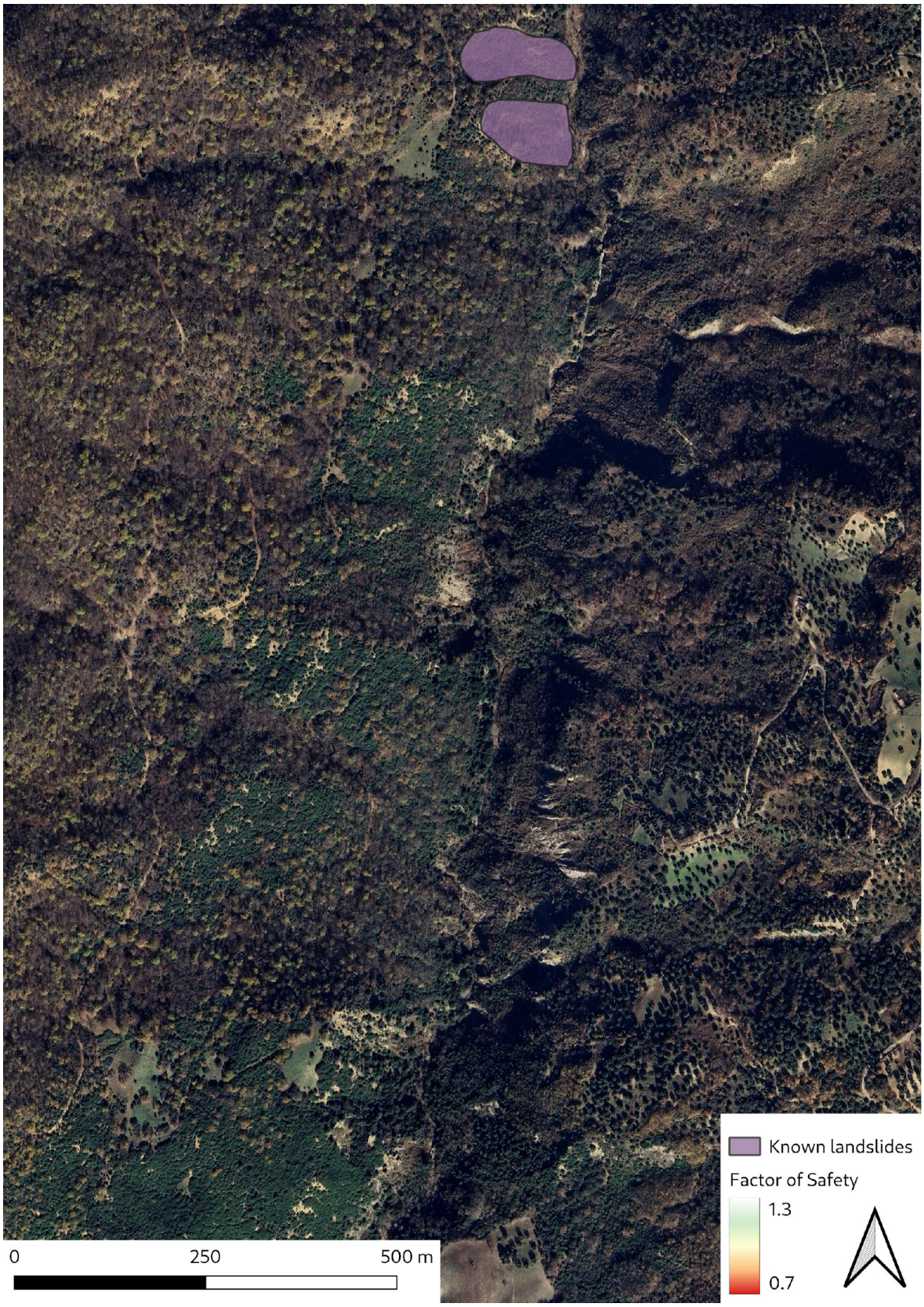

Figure 22. Satellite view of the valley located southwest of Stigliano. The area corresponds to that shown in Figure 21 and provides a preliminary visual feedback on the calculated factor of safety.

References

Amato, G., Fiorucci, M., Martino, S., Lombardo, L., & Palombi, L. (2023). Earthquake-triggered landslide susceptibility in Italy by means of Artificial Neural Network. Bulletin of Engineering Geology and the Environment, 82(5), 160. https://doi.org/10.1007/s10064-023-03163-x

Andresen, K.J., Huuse, M., Clausen, O.R., 2008. Morphology and distribution of Oligocene and Miocene pockmarks in the Danish North Sea - implications for bottom current activity and fluid migration. Basin Research, 20, 445-466.

Azhideh, S., Barani, S., Ferretti, G., & Scafidi, D. (2024). Earthquake-Induced Landslides in Italy: Evaluation of the Triggering Potential Based on Seismic Hazard. Applied Sciences, 14(8), 3435. https://doi.org/10.3390/app14083435

Baxter, P. J., Neri, A., & Todesco, M. (1998). Physical modelling and human survival in pyroclastic flows. Natural Hazards, 17(2), 163–176. https://doi.org/10.1023/

Boni, M. P., Faiella, A., Gazzola, V., & Pergalani, F. (2025). A multi-hazard and multi-risk assessment methodological approach to support Civil Protection planning in wide areas. International Journal of Disaster Risk Reduction, 119, 105343. https://doi.org/10.1016/j.ijdrr.2025.105343

Boulanger, R.W., Idriss, I.M., 2014. CPT and SPT based liquefaction triggering procedures. Report No. UCD/CGM.-14, 1, 134.

Bragato, P. L., Comelli, P., Saraò, A., Zuliani, D., Moratto, L., Poggi, V., Rossi, G., Scaini, C., Sugan, M., Barnaba, C., Bernardi, P., Bertoni, M., Bressan, G., Compagno, A., Del Negro, E., Di Bartolomeo, P., Fabris, P., Garbin, M., Grossi, M., … Parolai, S. (2021). The OGS–Northeastern Italy Seismic and Deformation Network: Current Status and Outlook. Seismological Research Letters, 92(3), 1704–1716. https://doi.org/10.1785/0220200372

Brodsky, E.E., Kanamori, H., 2001. Elastohydrodynamic lubrication of faults. Journal of Geophysical Research: Solid Earth, 106(B8), 16357-16374.

Brothers, L.L., Kelley, J.T., Belknap, D.F., Barnhardt, W.A., Andrews, B.D., Legere, C., Hughes Clarke, J.E., 2012. Shallow stratigraphic control on pockmark distribution in north temperate estuaries. Marine Geology.

Bussmann, I., Suess, E., 1998. Groundwater seepage in Eckernförde Bay (Western Baltic Sea): Effect on methane and salinity distribution of the water column. Continental shelf research, 18, 1795-1806.

Camerlenghi, A., Del Ben, A., Hübscher, C., Forlin, E., Geletti, R., Brancatelli, G., Micallef, A., Saule, M., Facchin, L., 2019. Seismic markers of the Messinian salinity crisis in the deep Ionian Basin. Basin Research.

Cattaneo, A., Miramontes, E., Samalens, K., Garreau, P., Caillaud, M., Marsset, B., Corradi, N., Migeon, S., 2017. Contourite identification along Italian margins: The case of the Portofino drift (Ligurian Sea). Marine and Petroleum Geology, 87, 137-147.

Ceramicola S., Tinti S., Zaniboni F., Praeg D., Planinsek P., Pagnoni G., Forlin E. (2014), Reconstruction and tsunami modeling of a submarine landslide on the Ionian margin of Calabria (Mediterranean Sea), K. Sassa, P. Canuti, Y. Yin (eds.), Landslide Science for a Safer Geoenvironment, Vol. 3, pp. 557-562, doi: 10.1007/978-3-319-04996-0_85, © Springer International Publishing Switzerland 2014.

Ceramicola, S., Dupré, S., Somoza, L., Woodside, J., 2018. Cold Seep Systems. In: A. Micallef, S. Krastel, A. Savini (Eds.), Submarine Geomorphology. Springer, Cham, pp. 367-387.

Chand, S., Knies, J., Baranwal, S., Jensen, H., Klug, M., 2014. Structural and stratigraphic controls on subsurface fluid flow at the Veslemøy High, SW Barents Sea. Marine and Petroleum Geology, 57, 494-508.

Cioni, R., Levi, S., & Sulpizio, R. (2000). Apulian Bronze Age pottery as a long-distance indicator of the Avellino Pumice eruption (Vesuvius, Italy).

Cox, S.F., 2016. Injection-driven swarm seismicity and permeability enhancement: Implications for the dynamics of hydrothermal ore systems in high fluid-flux, overpressured faulting regimes - An invited paper. Economic Geology, 111, 559-587.

Costa, A., Folch, A., & Macedonio, G. (2013). Density-driven transport in the umbrella region of volcanic clouds: Implications for tephra dispersion models. Geophysical Research Letters, 40(18), 4823-4827.

Della Seta, M.; Di Martino, G.; Esposito, C.; Giannini, L.M.; Martini, G.; Martino, S.; Pallone, F.; Troiani, F. Application of the PARSIFAL approach for providing scenarios of earthquake-induced landslide in the Accumoli municipality. In Proceedings of the GNGTS 2017 Conference, Trieste, Italy, 14–16 November 2017.

Del Gaudio, V., & Wasowski, J. (2011). Advances and problems in understanding the seismic response of potentially unstable slopes. Engineering Geology, 122(1–2), 73–83. https://doi.org/10.1016/j.enggeo.2010.09.007

Dellino, P., Mele, D., Sulpizio, R., Volpe, L. La, & Braia, G. (2008). A method for the calculation of the impact parameters of dilute pyroclastic density currents based on deposit particle characteristics. Journal of Geophysical Research: Solid Earth, 113(B7).

Dellino, P., Dioguardi, F., Doronzo, D. M., & Mele, D. (2019). The rate of sedimentation from turbulent suspension: An experimental model with application to pyroclastic density currents and discussion on the grain-size dependence of flow runout. Sedimentology, 66(1), 129-145.

Dellino, P., Dioguardi, F., Doronzo, D. M., & Mele, D. (2020). A discriminatory diagram of massive versus stratified deposits based on the sedimentation and bedload transportation rates. Experimental investigation and application to pyroclastic density currents. Sedimentology, 67(4), 2013-2039.

Di Trapani, F., Oddo, M. C., Sberna, A. P., & La Mendola, L. (2024). Structural health monitoring of masonry structures using stress sensors: Experimental induced damage tests and proposed approach for real-time monitoring. Construction and Building Materials, 449, 138077. https://doi.org/10.1016/j.conbuildmat.2024.138077

Dimitrov, L., Woodside, J., 2003. Deep sea pockmark environments in the eastern Mediterranean. Marine Geology, 195, 263-276.

Doronzo, D. M., & Dellino, P. (2011). Interaction between pyroclastic density currents and buildings: numerical simulation and first experiments. Earth and Planetary Science Letters, 310(3-4), 286-292.

Fader, G.B.J., 1991. Gas-related sedimentary features from the eastern Canadian continental shelf. Continental Shelf Research, 11, 1123-1153.

Foland, S.S., Maher, N., Yun, J.W., 1999. Pockmarks along the Californian Continental Margin: implications for fluid flow. Aapg Bull, 83, 681-706.

Folch, A., Mingari, L., Gutierrez, N., Hanzich, M., Macedonio, G., and Costa, A. (2020). FALL3D-8.0: a computational model for atmospheric transport and deposition of particles, aerosols and radionuclides – Part 1: Model physics and numerics, Geosci. Model Dev., 13, 1431–1458, https://doi.org/10.5194/gmd-13-1431-2020,

Garcia-Garcia, A., Orange, D., Lorenson, T., Radakovitch, O., Tesi, T., Miserocchi, S., Berne, S., Friend, P.L., Nittrouer, C., Normand, A., 2006. Shallow gas off the Rhône prodelta, Gulf of Lions. Marine Geology, 234, 215-231.

Gay, A., Berndt, C., 2007. Cessation/reactivation of polygonal faulting and effects on fluid flow in the Voring Basin, Norwegian Margin. Journal of the Geological Society, 164, 129-141.

Guerrichio, A. (1992). Convivere con i Grandi Movimenti di Massa - Lezione ad invito.

Guzzetti, F., Gariano, S. L., Peruccacci, S., Brunetti, M. T., Marchesini, I., Rossi, M., & Melillo, M. (2020). Geographical landslide early warning systems. Earth-Science Reviews, 200, 102973. https://doi.org/10.1016/j.earscirev.2019.102973

Guzzetti, F., Gariano, S. L., Peruccacci, S., Brunetti, M. T., & Melillo, M. (2022). Rainfall and landslide initiation. In Rainfall (pp. 427–450). Elsevier. https://doi.org/10.1016/B978-0-12-822544-8.00012-3

Hammer, Ø., Webb, K.E., 2010. Piston coring of Inner Oslofjord pockmarks, Norway: constraints on age and mechanism. Norwegian Journal of Geology/Norsk Geologisk Forening, 90.

Hasiotis, T., Papatheodorou, G., Kastanos, N., Ferentinos, G., 1996. A pockmark field in the Patras Gulf (Greece) and its activation during the 14/7/93 seismic event. Marine Geology, 130(3-4), 333-344.

Hersbach H, Bell B, Berrisford P, et al. (2020) The ERA5 global reanalysis. Q J R Meteorol Soc. 146: 1999–2049. https://doi.org/10.1002/qj.3803

Hill, J.M., Halka, J.P., Conkwright, R., Koczot, K., Coleman, S., 1992. Distribution and effects of shallow gas on bulk estuarine sediment properties. Continental Shelf Research, 12, 1219-1229.

Ho, S., Cartwright, J.A., Imbert, P., 2012. Vertical evolution of fluid venting structures in relation to gas flux, in the Neogene-Quaternary of the Lower Congo Basin, Offshore Angola. Marine Geology, 332-334, 40-55.

Ho, S., Hovland, M., Blouet, J.P., Wetzel, A., Imbert, P., Carruthers, D., 2018. Formation of linear planform chimneys controlled by preferential hydrocarbon leakage and anisotropic stresses in faulted fine-grained sediments, offshore Angola. Solid Earth, 9, 1437-1468.

Hovland, M., 2002. On the self-sealing nature of marine seeps. Continental Shelf Research, 22, 2387-2394.

Hovland, M., Gardner, J.V., Judd, A.G., 2002. The significance of pockmarks to understanding fluid flow processes and geohazards. Geofluids, 2, 127-136.

Hovland, M., Judd, A.G., 1988. Seabed pockmarks and seepages: impact on geology, biology and the marine environment.

Hovland, M., Judd, A.G., King, L.H., 1984. Characteristic features of pockmarks on the North Sea Floor and Scotian Shelf. Sedimentology, 31, 471-480.

Iannacone, L., Otárola, K., Gentile, R., & Galasso, C. (2024). Simulating multi-hazard event sets for life cycle consequence analysis. Natural Hazards and Earth System Sciences, 24(5), 1721–1740. https://doi.org/10.5194/nhess-24-1721-2024

Iglesias, J., Ercilla, G., García-Gil, S., Judd, A.G., 2010. Pockforms: an evaluation of pockmark-like seabed features on the Landes Plateau, Bay of Biscay. Geo-Marine Letters, 30, 207-219.

Ingrassia, M., Martorelli, E., Bosman, A., Macelloni, L., Sposato, A., Chiocci, F.L., 2015. The Zannone Giant Pockmark: First evidence of a giant complex seeping structure in shallow-water, central Mediterranean Sea, Italy. Marine Geology, 363, 38-51.

Iwasaki, T., Tokida, K., Tatsuoka, F., Watanbe, S., Yasuda, S. and Sato, H. (1982) Microzonation for Soil Liquefaction Potential Using Simplified Methods. Proceedings of the 3rd International Conference on Microzonation, Seattle, June 28-July 1, 1982.

Judd, A., Hovland, M., 2007. Seabed Fluid Flow: The Impact on Geology , Biology and the Marine Environment. Cambridge University Press, Cambridge.

Keefer, D. K. (1984). Landslides caused by earthquakes.

Kriebel D. L., Lynett P. J., Cox D. T., Petroff C. M., Robertson I. N., Chock G. Y. (2017). Energy method for approximating overland tsunami flows. Journal of Waterway, Port, Coastal, and Ocean Engineering, 143(5), 04017014. https://doi.org/10.1061/(ASCE)WW.1943-5460.0000393.

Lo Iacono, C.L., Sulli, A., Agate, M., Lo Presti, V., Pepe, F., Catalano, R., 2011. Submarine canyon morphologies in the Gulf of Palermo (Southern Tyrrhenian Sea) and possible implications for geo-hazard. Marine Geophysical Research, 32, 127-138.

Lube, G., Breard, E. C., Esposti-Ongaro, T., Dufek, J., & Brand, B. (2020). Multiphase flow behaviour and hazard prediction of pyroclastic density currents. Nature Reviews Earth & Environment, 1(7), 348-365.

Margheriti, L. (2021). Seismic Surveillance and Earthquake Monitoring in Italy.

Martino, S.; Battaglia, S.; Delgado, J.; Esposito, C.; Martini, G.; Missori, C. Probabilistic Approach to Provide Scenarios of Earthquake-Induced Slope Failures (PARSIFAL) Applied to the Alcoy Basin (South Spain). Geosciences 2018, 8, 57.

Martino, S., Battaglia, S., D'Alessandro, F. et al. Earthquake-induced landslide scenarios for seismic microzonation: application to the Accumoli area (Rieti, Italy). Bull Earthquake Eng 18, 5655–5673 (2020). https://doi.org/10.1007/s10518-019-00589-1.

Massaro, S., Stocchi, M., Martínez Montesinos, B., Sandri, L., Selva, J., Sulpizio, R., Giaccio, B., Moscatelli, M., Peronace, E., Nocentini, M., Isaia, R., Titos Luzón, M., Dellino, P., Naso, G., and Costa, A. (2023). Assessing long-term tephra fallout hazard in southern Italy from Neapolitan volcanoes, Nat. Hazards Earth Syst. Sci., 23, 2289–2311, https://doi.org/10.5194/nhess-23-2289-2023, 2023.

Mergili, M., Marchesini, I., Alvioli, M., Metz, M., Schneider-Muntau, B., Rossi, M., & Guzzetti, F. (2014). A strategy for GIS-based 3-D slope stability modelling over large areas. Geoscientific Model Development, 7(6), 2969–2982. https://doi.org/10.5194/gmd-7-2969-2014

Mergili, M., Marchesini, I., Rossi, M., Guzzetti, F., & Fellin, W. (2014). Spatially distributed three-dimensional slope stability modelling in a raster GIS. Geomorphology, 206, 178–195. https://doi.org/10.1016/j.geomorph.2013.10.008

Micallef, A., Spatola, D., Caracausi, A., Italiano, F., Barreca, G., D'Amico, S., Petronio, L., Coren, F., Facchin, L., Blanos, R., Pavan, A., Paganini, P., Taviani, M., 2019. Active degassing across the Maltese Islands (Mediterranean Sea) and implications for its neotectonics. Marine and Petroleum Geology, 104.

Montesinos B.M., Luzón M.T., Sandri L., Rudyy O., Cheptsov A., Macedonio G., Folch A., Barsotti S., Selva J., and Costa A. (2022) On the feasibility and usefulness of high-performance computing in probabilistic volcanic hazard assessment: An application to tephra hazard from Campi Flegrei. Front. Earth Sci. 10:941789. doi: 10.3389/feart.2022.941789

Neglia, F., Sulpizio, R., Dioguardi, F., & Sarocchi, D. (2023). Investigating the effect of polydispersity on the dynamics of multiphase flows using computational fluid dynamics tools. International Journal of Multiphase Flow, 168, 104558.

Nickel, J.C., di Primio, R., Mangelsdorf, K., Stoddart, D., Kallmeyer, J., 2012. Characterization of microbial activity in pockmark fields of the SW-Barents Sea. Marine Geology, 332, 152-162.

Noda A. et al. (2013) - Mass transport-dominated sedimentation in a foreland basin, the Hidaka Trough, northern Japan. Geochemistry Geophysics Geosystems (G3), 14, 2638–2660, doi:10.1002/ggge.20169

NTC, 2018. Norme tecniche per le costruzioni. Decree of the Minister of the Infrastructures, 42.

Paolucci, R., Near-source ground motion from normal faults: insights from the physics-based numerical simulations of the 1980 Irpinia earthquake, Southern Italy. Submitted to Earthquake spectra.

Picozzi, M., Zollo, A., Brondi, P., Colombelli, S., Elia, L., & Martino, C. (2015). Exploring the feasibility of a nationwide earthquake early warning system in Italy. Journal of Geophysical Research: Solid Earth, 120(4), 2446–2465. https://doi.org/10.1002/2014JB011669

Pecoraro, G., Calvello, M., & Piciullo, L. (2019). Monitoring strategies for local landslide early warning systems. Landslides, 16(2), 213–231. https://doi.org/10.1007/s10346-018-1068-z

Pecoraro, G., & Calvello, M. (2021). Integrating local pore water pressure monitoring in territorial early warning systems for weather-induced landslides. Landslides, 18(4), 1191–1207. https://doi.org/10.1007/s10346-020-01599-w

Picard, K., Radke, L.C., Williams, D.K., Nicholas, W.A., Siwabessy, P.J., Howard, F.J.F., Gafeira, J., Przeslawski, R., Huang, Z., Nichol, S., 2018. Origin of high density seabed pockmark fields and their use in inferring bottom currents. Geosciences, 8(6), 195.

Piciullo, L., Tiranti, D., Pecoraro, G., Cepeda, J. M., & Calvello, M. (2020). Standards for the performance assessment of territorial landslide early warning systems. Landslides, 17(11), 2533–2546. https://doi.org/10.1007/s10346-020-01486-4

Pickrill, R.A., 1993. Shallow seismic stratigraphy and pockmarks of a hydrothermally influenced lake, Lake Rotoiti, New Zealand. Sedimentology, 40, 813-828.

Pilcher, R., Argent, J., 2007. Mega-pockmarks and linear pockmark trains on the West African continental margin. Marine Geology, 244, 15-32.

Pittore, M., Cocussioni, S., Terzi, S., De Angeli, S., Cattari, S., Polese, M., Tocchi, G., Pozza, L., & Ferretti, F. (2023). Event-based multihazard and multi-risk storylines in RETURN.

Pokharel, B., Alvioli, M., & Lim, S. (2021). Assessment of earthquake-induced landslide inventories and susceptibility maps using slope unit-based logistic regression and geospatial statistics. Scientific Reports, 11(1), 21333. https://doi.org/10.1038/s41598-021-00780-y

Prestininzi, A., & Romeo, R. (2000). Earthquake-induced ground failures in Italy. Engineering Geology, 58(3–4), 387–397. https://doi.org/10.1016/S0013-7952(00)00044-2

Rise, L., Sættem, J., Fanavoll, S., Thorsnes, T., Ottesen, D., Bøe, R., 1999. Sea-bed pockmarks related to fluid migration from Mesozoic bedrock strata in the Skagerrak offshore Norway. Marine and Petroleum Geology, 16, 619-631.

Salvatore, M., Patrizia, C., Matteo, F., & Marco, M. G. (2020). Il Catalogo CEDIT: dall'inventario degli effetti sismoindotti all'analisi di scenario.

Sandri, L., Costa, A., Selva, J. et al. (2016) Beyond eruptive scenarios: assessing tephra fallout hazard from Neapolitan volcanoes. Sci Rep 6, 24271. https://doi.org/10.1038/srep24271

Seed, H.B., Idriss, I.M., 1971. Simplified procedure for evaluating soil liquefaction potential. Journal of the Soil Mechanics and Foundations division, 97, 1249-1273.

Shao, X., & Xu, C. (2022). Earthquake-induced landslides susceptibility assessment: A review of the state-of-the-art. Natural Hazards Research, 2(3), 172–182. https://doi.org/10.1016/j.nhres.2022.03.002

Skempton, A.W. and DeLory, F.A. (1957) Stability of natural slopes in London clay. In Proceedings of the 4th International Conference on Soil Mechanics and Foundation Engineering, vol. 2, pp. 378–381, London

Soter, S., 1999. Macroscopic seismic anomalies and submarine pockmarks in the Corinth–Patras rift, Greece. Tectonophysics, 308(1-2), 275-290.

Spatola, D., Hovland, M.T., Casalbore, D., Rovere, M., Chiocci, F.L., Dupré, S., Ercilla, G., Micallef, A., Papatheodorou, G., Sulli, A., 2025a. Pockmark Distribution and Genesis in the Mediterranean and Black Seas: A Regional Synthesis. Geosciences (2076-3263), 15(12).

Spatola, D., Rovere, M., Casalbore, D., Chiocci, F.L., 2025b. Pockmarks of the Mediterranean region seas: A Comprehensive Geodatabase for Marine Geomorphological Analysis. Scientific Data, 12(1), 1-7.

Sultan N. et al. (2004) - Triggering mechanisms of slope instability processes and sediment failures on continental margins: a geotechnical approach, Marine Geology, 213(1–4), 291– 321, doi:10.1016/j.margeo.2004.10.011

Szpak, M.T., Monteys, X., O'Reilly, S., Simpson, A.J., Garcia, X., Evans, R.L., Allen, C.C.R., McNally, D.J., Courtier-Murias, D., Kelleher, B.P., 2012. Geophysical and geochemical survey of a large marine pockmark on the Malin Shelf, Ireland. Geochemistry, Geophysics, Geosystems, 13, 1-18.

Tagarelli, V., & Cotecchia, F. (2025). Weather-Induced Landslide Activity in Clayey Slopes: Modeling for the Design of Site-Scale Early Warning Systems. Journal of Geotechnical and Geoenvironmental Engineering, 151(9), 04025092. https://doi.org/10.1061/JGGEFK.GTENG-13248

UNDRR. (2009). UNISDR terminology on disaster risk reduction. UN agency for the coordination of disaster risk reduction.

Valentine, G. A. (1998). Damage to structures by pyroclastic flows and surges, inferred from nuclear weapons effects. Journal of Volcanology and Geothermal Research, 87(1–4), 117–140. https://doi.org/10.1016/S0377-0273(98)00094-8

Vicari, A., Famiglietti, N. A., Colangelo, G., & Cecere, G. (2019). A comparison of multi temporal interferometry techniques for landslide susceptibility assessment in urban area: An example on stigliano (MT), a town of Southern of Italy. Geomatics, Natural Hazards and Risk, 10(1), 836–852. https://doi.org/10.1080/19475705.2018.1549113

Wald, D. J. (2020). Practical limitations of earthquake early warning. Earthquake Spectra, 36(3), 1412–1447. https://doi.org/10.1177/8755293020911388

Youd, T.L., & Perkins, D.M., 1978. Mapping liquefaction-induced ground failure potential. Journal of the Geotechnical Engineering Division, 104, 433-446.

Yu, K., Miramontes, E., Alves, T.M., Li, W., Liang, L., Li, S., Zhan, W., Wu, S., 2021. Incision of submarine channels over pockmark trains in the South China Sea. Geophysical Research Letters, 48(24), e2021GL092861.

Zhang, G., Robertson, P.K., & Brachman, R.W., 2002. Estimating liquefaction-induced ground settlements from CPT for level ground. Canadian Geotechnical Journal, 39, 1168-1180.

Zhu, S., Li, X., Zhang, H., Sha, Z., Sun, Z., 2020. Types, characteristics, distribution, and genesis of pockmarks in the South China Sea: insights from high-resolution multibeam bathymetric and multichannel seismic data. International Geology Review, 1-21.